SENCKENBERG

ORIGINAL PAPER

Palaeoenvironmental reconstruction of a coal bearing unit: the Upper Triassic Nayband Formation, Tabas Block, East-Central Iran

Ziba Zamani [1] · Hossain Rahimpour-Bonab[1] · Ralf Littke[2]

Abstract

The Qadir coal-bearing member of the Rhaetian Nayband Formation in the Parvadeh coal mine, East-Central Iran, was investigated for palaeoenvironmental reconstruction to predict coal properties. Along with field studies, rock petrography, XRD, and SEM-EDX analyses were carried out, and petrofacies, lithofacies, and facies associations were defined in a sequence stratigraphic framework. These studies represent a river-dominated, storm- and wave-influenced coastal/delta plain setting that accumulated along the shallow marine environment. The studied Qadir member is part of a paralic system that consists of progradational delta grading into shallow marine siliciclastic shelf sediments. Apart from sea-level fluctuations, the sedimentary pattern was mainly governed by tectonic events in a post-orogenic foreland setting connected to the rising Cimmerian Mountain range in the north. Sedimentological analysis and stacking patterns of the Qadir member indicate that discrete coal seam and zones in the member were formed by peat mires that extended onto the delta plain and occurred in fourth-order sequences stacked in the transgressive system tracts of the lower sequence (TST1) and early highstand systems tract of the upper sequence (HST2). However, the main economic coal zone was formed in the lower delta plain environment, predominantly within the middle part of the TST. The detrital nature and composition of the numerous partings and high ash content in the coal seams indicate that the coal-forming environment was a low-lying, topogenous flow-fed mire near detrital sources (i.e. distributary channels). Seemingly, coal layers are thicker with less sulfur (pyrite), but more ash toward the western part of the area.

Keywords Sequence Stratigraphy · Facies analysis · Palaeoenvironment · Upper Triassic · Nayband Formation · Tabas Block

Introduction

Most facies models of coal-forming mires indicate that peat accumulation is closely associated with clastic, fluvio-deltaic depositional environments in humid climates (Fielding 1987; Hagelskamp et al. 1988; Diessel 1992; McCabe 1993). Variation in depositional environments strongly influences peat composition, mainly ash and sulfur content and thickness (Ryer 1983; Fielding 1987; Hagelskamp et al. 1988; McCabe 1993; Flint et al. 1995; Bohacs and Suter 1997; Thomas 2002; Littke and Zieger 2019). The principal economic

features of coals are their thickness, lateral continuity, geometry, rank, and maceral and mineral content. Apart from rank, which is governed by burial related to the tectonic history, the remaining parameters are determined by factors controlling the peat mire; therefore, palaeoenvironmental studies are most helpful in predicting the coal properties.

Thus, predictions about the economic qualities of coal are feasible knowing the facies associations, the depositional systems, and the detailed stratigraphy of a coal-bearing succession. This is particularly important for neighboring areas with proven coal extension, which is concealed beneath younger deposits or which may lack quantitative geological data. These studies help to determine the best sites for drilling and reduction in exploration boreholes which to date is the main investigative tool for coal mining companies (Hagelskamp et al. 1988). Therefore, sedimentological and stratigraphic studies are essential from both an academic and an economic viewpoint.

✉ Hossain Rahimpour-Bonab
     rahimpor@ut.ac.ir

1   School of Geology, College of Science, University
     of Tehran, Tehran 6619-14155, Iran

2   Energy and Mineral Resources (EMR), RWTH Aachen
     University, 52056 Aachen, Germany

Some studies on coal seams by geologists have been done with little or no regard to surrounding clastic sediments (e.g. Hagelskamp et al. 1988; McCabe 1993), whereas the formation, development, and stratigraphic position of the peat swamp system is primarily controlled by the exactly the same mechanisms as clastic sediment deposition (Banerjee et al. 1996). This approach links strongly to changes in base-level as a driving force for peat/coal facies evolution (Bohacs and Suter 1997). Hence, for the first time, the coal-bearing Qadir member of the Nayband Formation in East-Central Iran (Fig. 1) has been investigated sedimentologically within a sequence stratigraphic framework.

Location and geological settings

The study area, i.e. the Parvadeh coal mine, is located within the Tabas Block, in the Central-East Iranian Microcontinent (CEIM), which was introduced by Takin in 1972 for the first time (Fig. 1). This microcontinent is a segment of the Iran/Central Iran Plate (Davoudzadeh and Schmidt 1984), which in turn is part of the Cimmerian continent or terrain (Saidi et al. 1997; Besse et al. 1998) (Fig. 1a). The CEIM is composed of three north-south oriented structural units, called Lut, Tabas and Yazd blocks from east to west, respectively (Fig. 1a). All of these blocks are separated by linear to curvilinear north-south right lateral strike-slip active faults. The Tabas Block is an intracontinental depression with a spindle shape and is constrained by the active Nayband Fault in the east and Kalmard-Kuhebanan Fault in the west (Konon

et al. 2016). Some evidence, such as facies change and thickness of the formations, show that these faults were active during Triassic-Jurassic time (Seyed-Emami 2003). The Tabas Block contains a very thick and well-exposed Upper Triassic-Jurassic sequence (Fig. 1b). The main coal-bearing Qadir member in the Parvadeh coal mine has a well-exposed outcrop in this area that includes seven coal seams, i.e. A, B1, B2, C1, C2, D and E (Fig. 2b; Zamansani et al. 2019). At outcrop, the seams initially dip between 15° to 30° generally toward west but flatten to between 5° to 10° at 400-600 m below the surface (Shariat Nia 1994).

The Parvadeh coal mine, with an area of 1200 km^2, is located west of the southern Khorasan Province, about 75 km south of Tabas City. This area is bounded by the Cheshmeh Rostam and Quri Chay faults to the north and south, respectively, Nayband Fault in the east and a hidden fault in the west (Fig. 2a). Nayband Fault and its splays such as Cheshmeh Rostam and Quri Chay, govern tectonism of the region (Shariat Nia 1994; Konon et al. 2016) (Figs. 1b, 2a). These faults are associated with smaller northeast-southwest trending strike-slip faults, which segment the area into discrete blocks. The region influenced by these strike-slip faults has been divided into smaller areas, which from west to east are termed Parvadeh I (PI), PII, PIII, PIV, and Eastern Parvadeh (PE), respectively (Fig. 2a). Proximal to these faults, a series of anticlines and synclines with east-west trending fold axes have developed and transform into monoclines near the faults. This low dipping (5° to 15° generally toward the south) monoclinal style has been preserved over extensive parts of the area and consequently has provided persistent
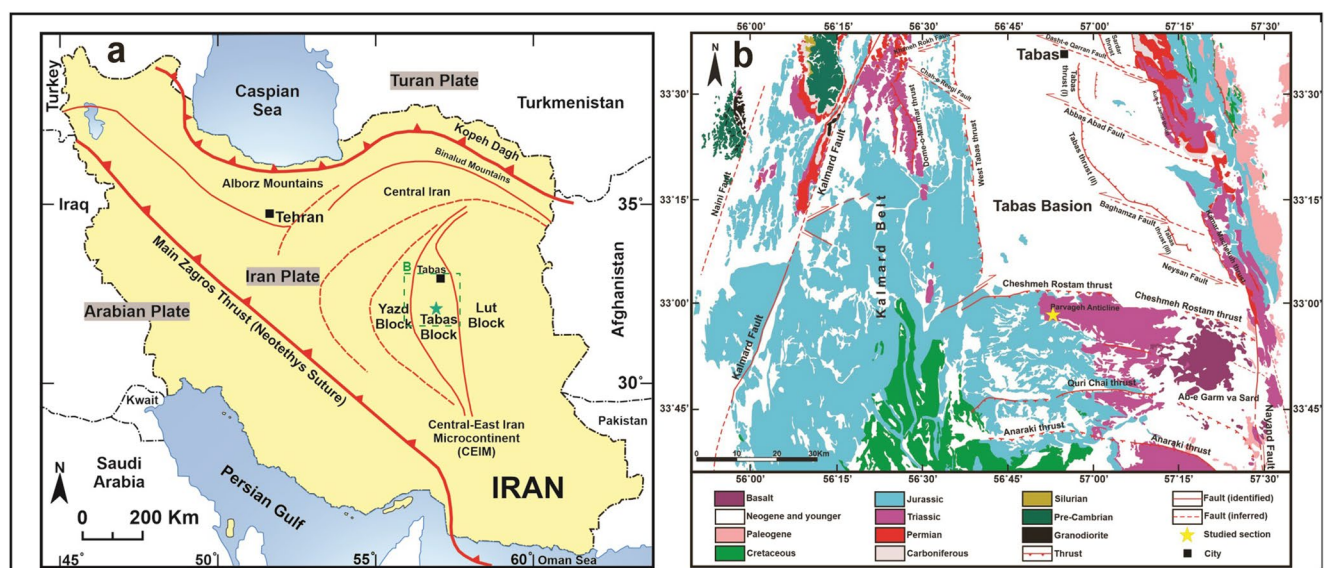

Fig. 1 **a** Simplified structural and geographical framework of Iran showing the main sutures, structural units and geographical area (redraw from Wilmsen et al. 2009b). Studied area is indicated by asterisk in the a and B figures, **b** Geological map from a part of northern Tabas Block (redraw from Konon et al. 2016)
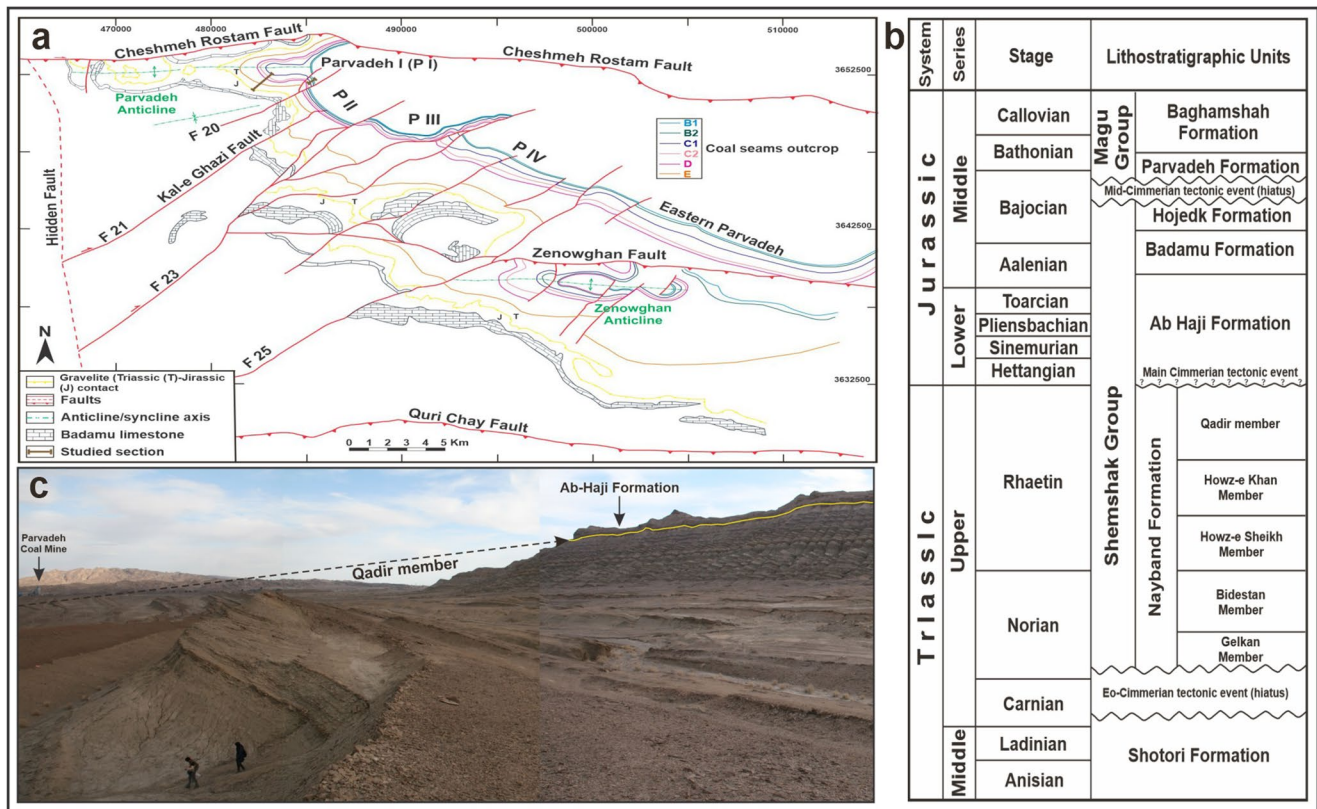
Fig. 2 **a** Structural blocks and coal seams outcrop in the Parvadeh Area (modified after Shariat Nia 1994 and Shariat Nia et al. 1997). Location of the studied section is indicated on the map, **b** Main lithostratigraphic units of the Middle Triassic to Middle Jurassic successions in the Parvadeh Area (Modified from Wilmsen et al. 2009a; Cirilli et al. 2005; Seyed-Emami et al. 2004, 2005; Seyed-Emami 2003), **c** Distance panorama field view of the Qadir coal-bearing measured section in the Parvadeh coalmine area, view is to the southeast

low dipping and relatively undisturbed mining blocks (Ghassabiyan et al. 2010)

Tectonics and palaeogeography

The structural history and sedimentary development of the Triassic in Iran are primarily governed by Cimmerian Orogeny (Seyed-Emami, 2003), which was first recognised in Iran by Stöcklin (1974). Structural, lithological, palaeontological, and palaeomagnetic investigations (e.g. Davoudzadeh and Schmidt,1984; Saidi et al.,1997; Besse et al.,1998; Fürsich et al.,2005; Muttoni,2009; Wilmsen et al. 2009a, b; Ghavidel-Syooki et al. 2015; Sajjadi et al. 2015) indicate that from the Precambrian to the Permian, the Central Iran Plate was a part of northern Gondwana and was separated from the Turan Plate (Laurasia) by the Paleo-Tethys Ocean (Davoudzadeh and Schmidt 1984; Seyed-Emami 2003). The Paleo-Tethys Ocean was narrowed and eventually destroyed by north-directed subduction below Eurasia from the Devonian onwards (Golonka 2007). After subduction of the Paleo-Tethys mid-ocean ridge system, the Iran Plate, as a coherent part of the Cimmerian Terrane, broke and detached from the northern margin of Gondwana during the middle to late Permian drifting toward Eurasia, which caused the Neo-Tethys Ocean to open at the expense of the Paleo-Tethys (Fig. 3a). The northward drift of the Iran Plate was completed at the beginning of the Late Triassic when the closure of the Paleo-Tethys and accretion to the southern margin of Eurasia (Turan Plate) initiated the Early Cimmerian Orogeny (Davoudzadeh and Schmidt 1984; Saidi et al. 1997; Besse et al. 1998; Wilmsen et al. 2009a, b; Ghassabiyan et al. 2010; Cifelli et al. 2013).

The continent-continent collision caused extensive uplift and created pronounced topographies along the Iranian Plate. At the northern margin of the plate, an underfilled Carnian-Rhaetian flexural foreland basin formed (Wilmsen et al. 2009a, b) (Fig. 3b). At the same time, Neo-Tethys subduction started at the southern margin of the Plate, which reduced compressional tectonics on the Iran Plate. With the subsequent formation of extensional subsiding basins and transgression of the sea onto the CEIM, these basins were filled, while areas of high elevation were strongly eroded. Thus about 3000 m of Nayband and other formations of the
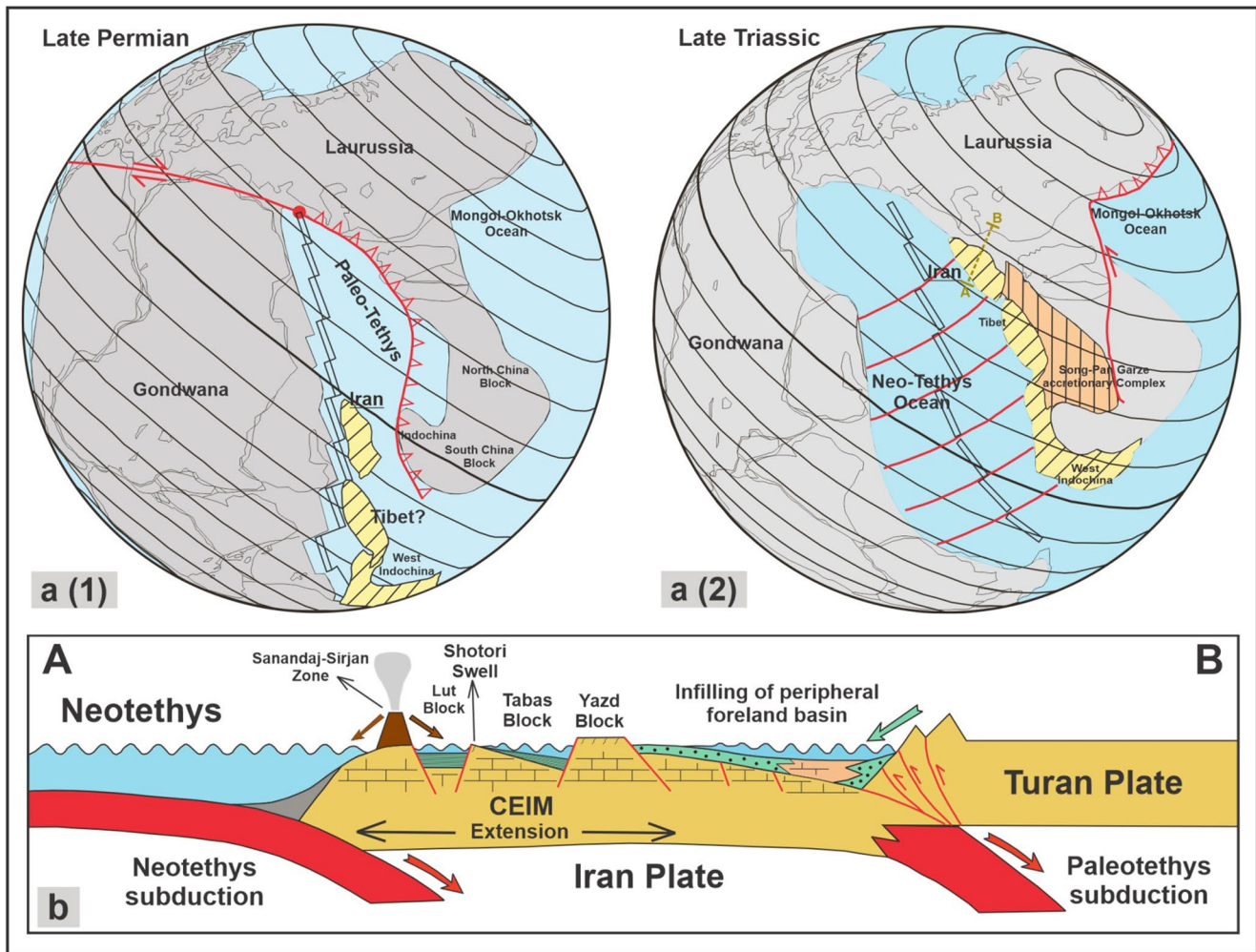
Fig. 3 Global palaeogeographic and geodynamic reconstruction map of: **a** The Tethyan Oceans and its bordering continents during the late Permian **a (1)** and the Late Triassic **a (2)** (Modified after Besse et al. 1998), cross-hatched areas represent Cimmerian Blocks, **b** Geody-namic sketch of the Late Triassic (middle Norian-Rhaetian) effects of the Cimmerian Orogeny on the Iran Plate, along A-B line in a (2) fig-ure (modified from Cifelli et al. 2013; Wilmsen et al. 2009b)

Shemshak Group (Fig. 2b) were deposited (Seyed-Emami 2003; Fürsich et al. 2005; Wilmsen et al. 2009b).

Stratigraphic architecture

Nayband Formation is well developed in the Tabas Block, whereas it is only present in some areas of the Lut Block and is absent in the Yazd Blok (Fürsich et al. 2005). These sediments post-date the Early Cimmerian tectonic event and overlie Middle Triassic carbonates of the Shotori Formation with an erosional unconformity and ancient karst (Kluyver et al. 1983).

Since the first study on the introduction and subdivision of the Nayband Formation by Douglas (1929), various stratigraphic, palaeontologic, and sedimentologic studies in Central Iran showed an outer ramp to the fluvial sedimentary

environment for this formation, which is of Norian to Rhae-tian age (Brönnimann et al. 1971; Kluyver et al. 1983; Repin 1996; Nützel and Senowbari-Daryan 1999; Seyed-Emami 2003; Fürsich et al. 2005; Hautmann et al. 2011; Ghavidel-Syooki et al. 2015; Bayet-Goll and Neto De Carvalho 2017; Krystyn et al. 2019; Etesampour et al. 2020; Sabbaghiyan et al. 2020).

According to Brönnimann et al. (1971), in the Nayband type section at the southern flank of the Nayband Moun-tain, this formation has a thickness of 2195 m and its overall thickness decreases towards the north (Fürsich et al. 2005). The formation is subdivided from bottom to top into the fol-lowing four members: 1) lower sandstone and shale member (Gelkan Member, 915 m); 2) middle limestone and shale member with common *Heterastridium*, an extinct marine Triassic hydrozoan (Bidestan Member, 450 m); 3) upper sandstone and shale member (Howz-e Sheikh Member, 365

m), and 4) upper member with alternations of limestone, shale, sandstone and prominent reefal structures with frequent sponges and corals (Howz-e Khan Member, 465 m) (Fig. 2b). In addition to these four formal members, further three informal members, composed of coal-bearing siliciclastic with thicknesses between 500-900 m, have been proposed by Kluyver et al. (1983). Further to the north, in the South Shotori Mountains (Kamar-e-Machekuh) and in the Parvadeh Area, the upper carbonate member (Howz-e Khan Member) is partly or entirely replaced by a thick, siliciclastic sequence with prominent coal measures, resulting from tectonic activities at this time. This unit has been named informally, by the geologists of the National Iranian Steel Company, as Qadir member (Shariat Nia 1994).

A complete section of the Qadir member is present in the Parvadeh Region, where its thickness exceeds 1000 m, with lithologies similar to the type section (Shariat Nia 1994). At the top of the Qadir member there is a clear-cut boundary with the overlying Ab-Haji Formation (Fig. 2c). At the base of fluvial sediments of the Ab-Haji Formation (Salehi et al. 2015), there are some coarse-grained sandstones with variable thickness constituting a micro-conglomerate termed the "Gravellite" horizon. The base of this bed was defined as the Triassic-Jurassic boundary (Shariat Nia 1994; Seyed-Emami 2003; Wilmsen et al. 2009a; Salehi et al. 2015). Salehi et al. (2015) proposed this coarse-grained horizone may have been caused by source area uplift due to slab break-off of the subducted Iran Plate in the course of the Cimmerian collision in CEIM. Investigation of the Late Triassic plant fossils concluded that the Qadir member and Ab-Haji Formation are not conformable, and there is a stratigraphic gap at this boundary (Shariat Nia 1994). According to palaeontological investigations in this area, the age of Qadir member is Rhaetian (Hautmann et al. 2011; Ghavidel-Syooki et al. 2015; Sabbaghiyan et al. 2020).

Sampling and analytical methods

A composite stratigraphic section of Qadir member with a total thickness of 507.3 m was measured, described, and sampled in the southeast and west of the Parvadeh Anticline (56° 48' 56" E, 33° 0' 27" N), where this member is accessible and exposed (Figs. 2a, c). The base of this section is covered and disconformably overlain by Ab-Haji Formation at the top (Figs. 2a, c).

The data gathered in the field include colour, size, texture, composition, lithology, thickness, fossils, trace fossils, weathering profile, nature of bedding, bed geometry, bed continuity, sedimentary structures, stratigraphic surface, lateral and vertical facies change, and transitions of sediments. Thin sections were prepared from a total of 70 rock samples, which were studied microscopically under polarized light for microfacies analysis. Lithofacies were defined based on sedimentary structures and lithology. Petrofacies description and classification of siliciclastic sediments was done according to Stow (1981) and Folk (1980), and for carbonates according to Embry and Klovan (1971). Ten lithofacies and six facies associations were established using the classification of Miall (2000, 2006). The facies associations were defined by stratal characteristics and groups of genetically related sets of sediments. For sequence stratigraphic interpretation, the concepts developed in earlier studies were considered (e.g. McCabe 1993; Banerjee et al. 1996; Bohacs and Suter 1997; Holz et al. 2002; Catuneanu 2003).

Eight rock samples were selected for X-ray diffraction (XRD) analysis to identify the type and amounts (semi-quantitative) of significant minerals (Table 1). This measurement was performed on sample powder using a Philips PW1800 diffractometer with Cu Kα radiation.

Another method applied was SEM because identifying minor minerals is difficult and inreliable due to XRD detection limits (generally at about 0.5-1%) and peak overlapping. This technique was also employed to characterise microstructures and the macro- and mesopore systems. Fresh surfaces of 8 samples were coated with gold powder and investigated using a TESCAN-VEGA II XMU instrument equipped with an energy dispersive X-ray analyzer (EDX). SEM-EDX analysis provides elemental data on small areas at minimum concentrations of 0.1-0.5 weight percent (wt%); thereby, the mineralogical composition of rock constituents could be established.

Petrofacies analysis

The petrographic study of thin sections (petrographic facies) showed that the main petrofacies of the sandstones are sublitharenite (often subchertarenite), rarely litharenite, and quartzarenite (Figs. 4a, 5). The petrofacies of fine-grained sediments change from claystone to siltstone (Figs. 5, 6). Monocrystalline quartz is predominant (Fig. 5), and its presence can be related to the recycling of older, quartz-rich rocks (especially with volcanic sources) followed by long-distance transportation in a high-energy regime (Tucker 2001; Boggs 2009).

Polycrystalline quartz, muscovite, and feldspar are other common minerals (Figs. 5a-b). Small amounts of feldspar and sericitized feldspar grains (Fig. 5d) can be related to a tropical climate during the Rhaetian time and thus intense feldspar alteration (Folk 1980). Minor minerals present in all petrofacies include zircon, glauconite, rutile, apatite, and pyrite (Fig. 5d). In some fine- and medium-grained samples, pyrite or iron oxide pseudomorphs (goethite) are visible (Figs. 6a, d). The small amounts of glauconite throughout the studied section can indicate shallow marine conditions

Table 1 Results of Bulk-XRD analysis of the siliciclastic samples

Sample name	Thickness (m)	Lithology	Minerals (wt.%)									
			Quartz	Calcite	Siderite	Kaolinite	Illite	Muscovite-illite	Chlorite	Gypsum	Hematite	Albite
QP 2	2	Silty claystone	41.8	0.0	0.0	15.3	28.6	0.0	0.0	0.0	0.0	14.3
QP 9	42.7	Siltstone	37.1	0.0	0.0	14.4	0.0	36.1	0.0	0.0	4.1	8.3
QP 24	144.4	Sublitharnite sandstone	51.6	10.3	0.0	0.0	0.0	13.4	14.4	1.0	0.0	9.3
QP 28	200.7	Silty shale	37.9	2.1	0.0	0.0	0.0	31.6	18.9	0.0	0.0	9.5
QP 38	259	Sublitharnite sandstone	56.9	6.3	0.0	0.0	0.0	13.7	10.5	0.0	0.0	12.6
QP 49	347.9	Sublitharnite sandstone	37.9	23.2	0.0	0.0	0.0	14.7	13.7	0.0	0.0	10.5
QP 51	382.5	Siltstone	40.8	2.0	0.0	0.0	0.0	23.5	16.3	0.0	0.0	17.4
QP 64	480.8	Silty sublitharnite sandstone	38.8	3.1	16.3	13.3	0.0	16.3	0.0	0.0	0.0	12.2
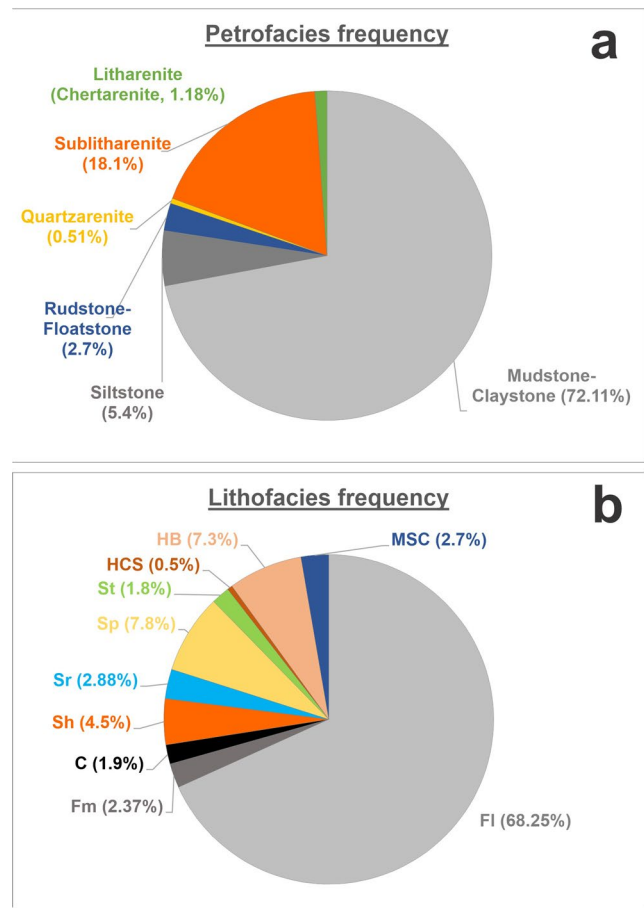
Fig. 4 Petrofacies (**a**) and lithofacies (**b**; see Table 2) frequency in the studied surface section of Qadir member

(Hagelskamp et al. 1988; Worden and Morad 2003). The main lithic fragments are chert, but at the top of the succession, metamorphic and sedimentary fragments (mudstone/shale, siltstone, and very fine-grained sandstone) are typical as well (Fig. 5b). Lithic fragments can be critical indicators of the tectonic activities and indicate relatively short transportation distances (Tucker 2001). Increasing lithic clasts at the top of the section may be due to uplift around the Triassic-Jurassic boundary (Wilmsen et al. 2009a, b), when recycling of older sedimentary and metamorphic rocks occurred.

Scattered coal fragments, palynomorphs, and fine- to coarse-grained bioclasts are visible in some sandstone layers. The percentage (vol%) of quartz grains in sandstone is variable (about 75-95%), rock fragments are at about 5 to 25%, and other grain minerals are about 1 to 5%. The grain size in sandstones is mostly very fine to fine, but limited medium-grained sandstone layers are visible at the top of the section (Fig. 7). These grains are usually medium to well-sorted and sub-angular to rounded (Fig. 5). At the top of the section up to 10% matrix is visible between the sandstone grains. Calcite and iron oxide are the main cement, but
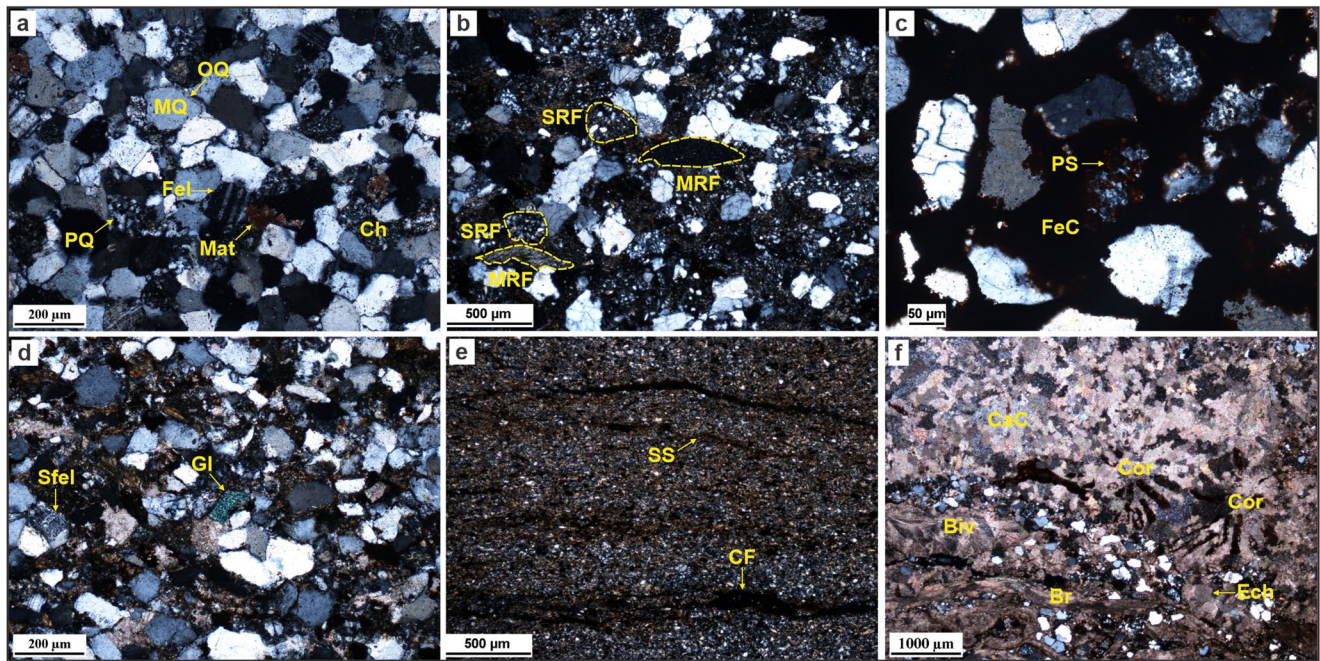
Fig. 5 Photomicrographs of the siliciclastic and carbonate petrofacies/microfacies of Qadir outcrop section (*XPL*), **a** Mature chertarenite with monocrystalline quartz (*MQ*), authigenic overgrowth quartz (*OQ*), polycrystalline quartz (*PQ*), chert grains (*Ch*) and patchy matrix (*Mat*), **b** Submature sedarenite with siltstone (*SRF*) and metamorphic (slate-schist) rock fragments (*MRF*), **c** Mature chertarenite with iron oxide cement (*FeC*) and oxidized pseudomorph of siderite crystals (*PS*), **d** Glauconite grain (*Gl*) and sericitized feldspar (*SFel*) in submature sedarenite. **e** Faint laminated siltstone with solution seam (*SS*) and coal fragments (*CF*), **f** Sandy rudstone with calcite cement (*CaC*), and micritized coarse coral (*Cor*), bivalve (*Bi*), brachiopod (*Br*) and echinoderm (*Ech*) bioclast

dolomite, ankerite, siderite, silica, barite, anhydrite, celestine, and pyrite as minor cements are also visible (Figs. 6a-d). The presence of barite, celestine, and pyrite cement may be due to the influence of seawater.

In addition to the siliciclastic facies, thin carbonate layers (shell beds) show sandy floatstone to rudstone facies (Fig. 5f). Bivalves, gastropods, brachiopods, echinoderms, corals, and rarely benthic foraminifers are the main bioclasts which are embedded in micrite matrix and calcite cement. They usually appear as molds filled with calcite cement (Fig. 5f). The allochems are cemented by blocky and drusy calcite cement. The distribution pattern of calcite cementation at parasequence boundaries is usually attributed to the increased amount of carbonate bioclasts and/or to the long residence time of the sediments at shallow depths below the sea floor (Ketzer et al., 2003).

A common feature of coal-bearing strata is the formation of ironstone as bands, nodules, and cement. Siderite is present mainly as nodules and cement in close proximity to the coal seams and seemingly is syngenetic (early diagenetic) in origin (Vassilev and Vassiliva 1996). The early diagenetic siderite typically indicates water-logged, organic-rich, sulfate-poor, and methanic environments (Gastaldo et al. 1993). It seems that siderite was the precursor mineral for iron-oxide cement. The association of siderite with this cement

and rhomb-shaped iron oxide pseudomorphs may indicate pre-existing siderite (Fig. 5c) (Burgess 2014). Also, pyrite crystals oxidized to goethite act as cement (Figs. 6a, d).

The clay minerals, which XRD and SEM-EDX distinguish, are kaolinite, illite, chlorite, and mixed layers (Fig. 6, Table 1). Besides the fine-grained sediments, these minerals occur in sandstones and carbonates. Illite and chlorite are the main clay minerals in the siliciclastic Qadir member. Illite and chlorite dominate the mesodiagenetic stage and usually grow at the expense of eodiagenetic clay minerals, detrital feldspars, and lithic grains (Worden and Morad 2003). Chlorite is usually present in marine shores rich in iron ions derived from rivers. Illite usually has a detrital origin in coal-bearing strata, although a certain proportion of illite is probably diagenetic as a weathering product of feldspar and muscovite (Vassilev and Vassiliva 1996).

Kaolinite is abundant in paralic and shallow marine environments (Worden and Morad, 2003; Burley and Worden, 2003). It often appears as pseudohexagonal plates that are commonly stacked in a book habit (Fig. 6b). Kaolinite forms under humid climatic conditions in continental sediments by the action of slightly acidic water on aluminosilicate minerals such as feldspars, mica, and pyroclastic glasses (Vassilev and Vassiliva 1996; Worden and Morad 2003). The tropical climate at the end of the Triassic (Vaez-Javadi 2012) may
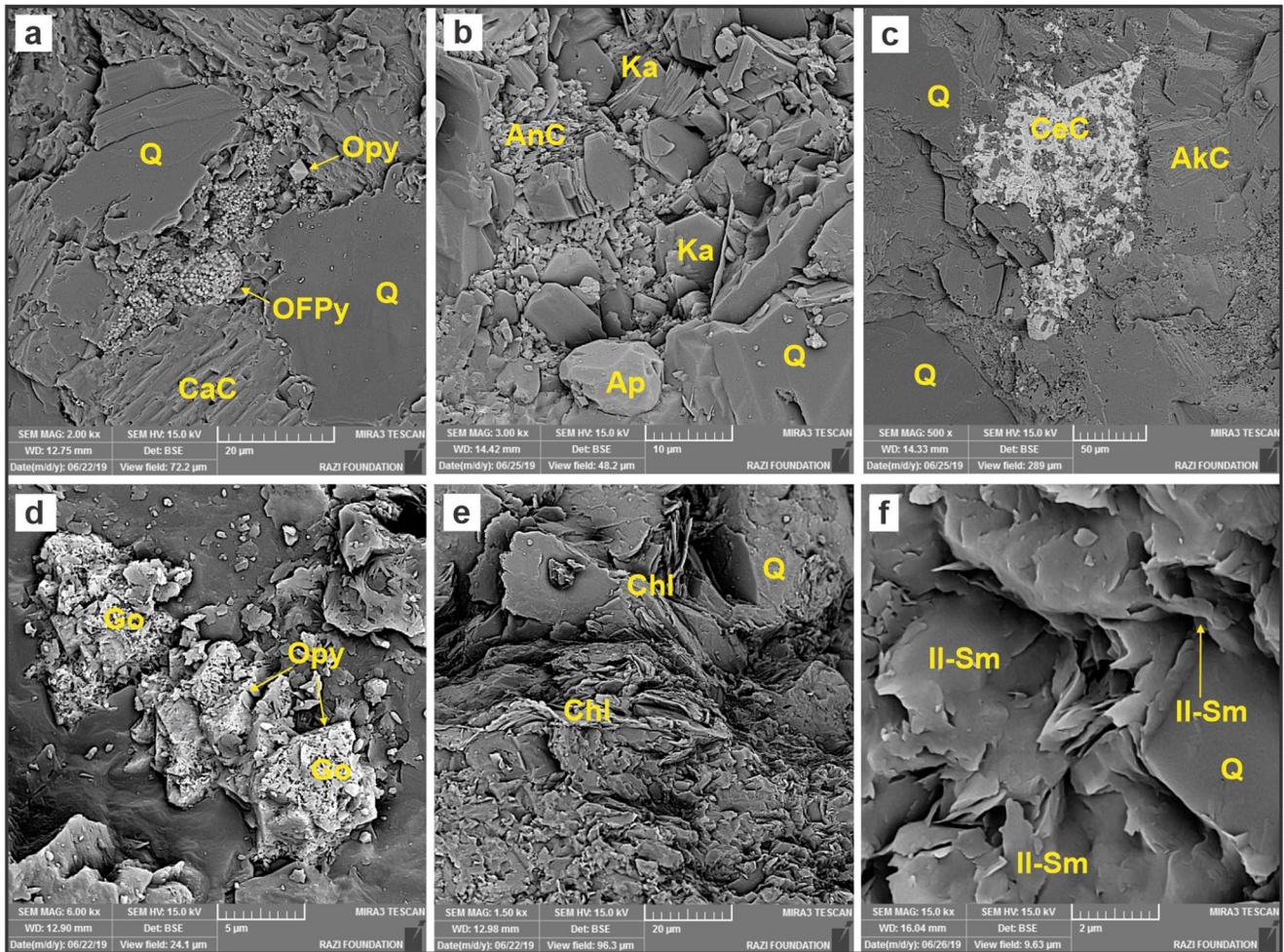
Fig. 6 Back scattered and secondary scanning electron microscopic (SEM) images exhibiting **a** Corroded detrital quartz grains (*Q*) by calcite cement (*CaC*), pore-filling oxidized framboidal pyrite (*OFPy*) and single octahedral pyrite (*OPy*) crystals (goethite), **b** Lath-like anhydrite cement (*AnC*), partly pore-filling, authigenic pseudohexagonal kaolinite (*Ka*) and detrital apatite grain (*Ap*), **c** Patchy celestite cement (*CeC*) and pore-filling rhombic ankerite crystals (*AkC*) between Q, **d** Oxidized pyrite (*OPy*), **e** Detrital chlorite lamina (*Chl*) with preferable orientation along quartz grains, **f** Mixed layer curly illite-smectite clays (*Il-Sm*) with flaky and slightly crenulated shape over and between detrital grains

have resulted in more significant amounts of meteoric waters and promoted eodiagenetic kaolinization. Also, permeable sandstones below subaerially exposed sequence boundaries were subjected to mechanical clay infiltration or pervasive kaolinization resulting from percolation of undersaturated meteoric water in a humid climate (Worden and Morad 2003; Ketzer et al. 2003).

Lithofacies

Based on field studies and microscopic petrography, ten lithofacies (LF) were identified within the studied succession (Figs. 4b, 7; Table 2). These LFs consist of two fine-grained LF (mudrocks), one biochemical LF (coal, C), five medium-grained LF (sandstones), and one heterolithic bedding LF (HB), and one mixed siliciclastic-carbonate LF (MSC). Fine-grained LF consists of horizontally laminated (Fl) and massive mudrock (Fm) LF. Medium-grained LF includes horizontally laminated (Sh), rippled cross-bedded (Sr), planar cross-bedded (Sp), trough cross-bedded (St), and hummocky cross-bedded sandstone (HCS).

Fine-grained lithofacies

Fine-grained LF is the most abundant facies and consists of about 70% of the studied section (Figs. 4b, 6) and was deposited in diffrent environments, from delta/coastal
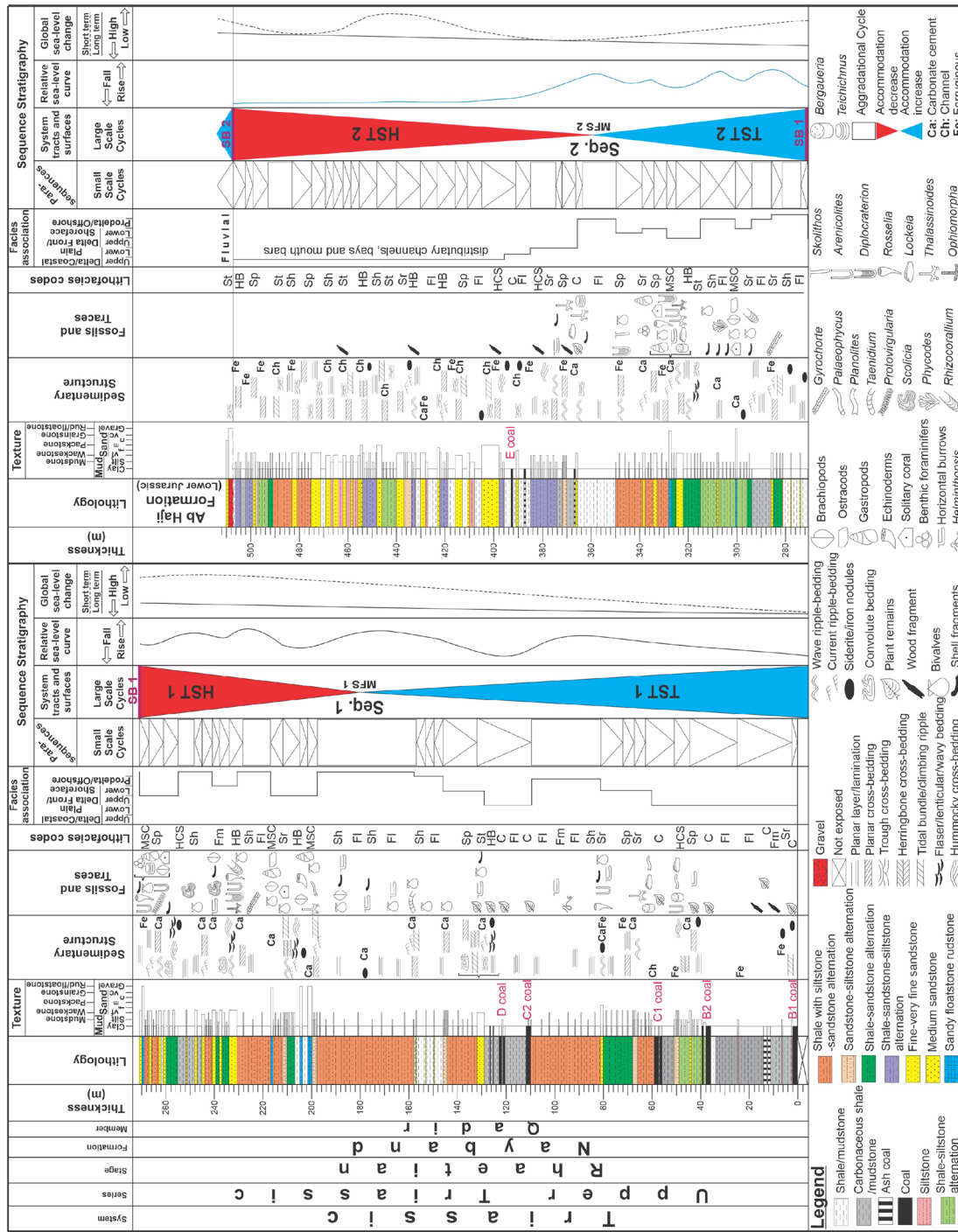
Fig. 7 Lithostratigraphic column of Qadir coal-bearing measured section in the Parvadeh Area showing the sedimentological characteristics, interpretation of depositional environments and sequence stratigraphy. Reconstructed sea-level curve is compared with the global curve (Haq 2018)

Table 2 Lithofacies description and interpretation of the studies Qadir member in the Parvadeh Area

Lithofacies code	Description	Lithology and petrofacies	Interpretation
Fl	Horizontally laminated mudrock, clay to silt size, light green to dark gray, usually is associated with Sh, Sr, C and Fm, 0.5 m to more than 30 m, sheet like body, sometimes with plant fossils and organic matter, gradual contact at the top and base	Claystone, mudstone, siltstone and shale	Deposition in low-energy environment from suspension, in delta/coastal plain, prodelta and offshore (Wight 1985)
Fm	Massive mudrock, clay to silt size, light green to dark gray, Accompanied with C and Fl, 0.5 to 1 m thickness, gradual contact at the base and top	Claystone, mudstone and siltstone	Rapid deposition from suspension in low-energy condition (Miall 2006; Boggs 2009), in delta/coastal plain, prodelta
C	Coal, black to very dark gray, organic rich, with lots of plant fossils, medium to high ash content, up to 3 m thickness, gradual contact at the base and sharp at top, more than 1% sulfur content	Coal and ash coal	Vegetated delta/coastal plain mires with marine incursion, sub to anoxic condition (Miall 2006)
Sh	Horizontally laminated sandstone, very fine to fine-grained sandstone, well sorted and rounded grains, gray to light gray, scattered pant fragments, up to 2 m thickness, sheet like to tabular geometry, usually alternates with Sr and Sp and laterally changes to them and Fl	Sandstone, sublitharenite, litharenite, chertarenite	Deposited under upper to low flow regime by unidirectional current and traction transport mechanism (Miall 2006; Boggs 2009) in shallow marine shelf, channels, delta plain and delta front
Sr	Rippled cross-laminated sandstone, very fine to fine sandstone, gray to light gray, well sorting and roundness grains, 5 to 30 Cm thickness, current and wavy ripples, locally climbing ripples and herringbone cross stratification, associated with Sh, Sp, Fl, sheet like geometry,	Sandstone, sublitharenite, chertarenite, quartzarenite	Formed under subaqueous traction of grains by unidirectional current or oscillatory low flow regime (Boggs 2009) in delta/coastal plain, channels and upper shoreface (Miall 2000, 2006; Davis 2012)
Sp	Planar cross-bedded sandstone, fine to very fine-grained sandstone, gray to reddish color, moderate to well sorted, rounded, alternate with Sh, Sr and St, 0.1 to 1 m thickness, tabular and wedge-shaped	Sandstone, sublitharenite	Deposited by migration of 2D ripple marks in unidirectional current in the low flow regime conditions (Miall 2006), close to river bank shallow marine, delta front and point bars
St	Trough cross-bedded sandstone, fine to medium-grained sandstone, light gray to gray, well sorted, medium to well-rounded grains, 0.3 to 3 m thickness, accompanied with Sr, HB and Sp, with lenticular to tabular geometry	Sandstone, litharenite, sublitharenite	Originated by migration of 3D bed forms in small current ripple or large-scale ripples (dunes) (Boggs 2009) under turbulent current or channel filling (Tucker 2001; Miall 2006), in channel, delta plain, delta front and upper shoreface
HCS	Hummocky cross-bedded sandstone, fines-grained sandstone, gray color, well sorted and rounded grains, accompanied with Sh, Sr and Sp, 0.15 to 0.4 m thickness, with lenticular geometry	Sandstone, litharenite, sublitharenite	formed by combination of unidirectional and oscillatory flows related to wave and storm, (Boggs 2009) in the shallow marine siliciclastic shelf and wave influenced lower delta front
HB	Heterolithic bedding, with clay, silt and very fine to fine-grained sand size, gray color, plant debris, 0.1 to 0.3 m thickness, alternation of Sr, Sh, Sp, Fl and Fm, with flaser, lenticular and wavy bedding	Mudstone, siltstone, shale, sandstone, sublitharenite	Formed by alternating strong and weak flows from coastal plain to offshore, mouth bar, channels and delta front
MSC	Mixed siliciclastic-carbonate, sandy to silty carbonate, gray to reddish color, fragments or body fossils of echinoderm, gastropod, coral, brachiopod and bivalve, negligible amounts of micrite matrix, 0.05 to 2.5 m thickness, laterally pinched out	Sandy rudstone, sandy floatstone, bioclastic sandstone	Formed in relatively high-energy upper shoreface to offshore transition and delta front to prodelta

planin to offshore. This LF includes clay and silt sizes of grains. Their thicknesses through the section change from millimetres to more than 40 m, and they prevail within the lower and middle parts of the section (Fig. 7). Dark and drab colours (grey, green, and brown) of this LF (especially near the coal layers) are due to presence of pyrite minerals and siderite nodules in some intervals (Figs. 8a, k), indicating its formation under reducing conditions (Miall 2006; Davis 2012). The co-existing pyrite and siderite in general were not usual; However if syngenetic siderite and pyrite were contemporaneously formed, this usually happened under neutral to weak alkaline under reducing conditions conditions (Dai et al., 2020).

Horizontally laminated mudrock lithofacies (Fl)

Mudrock intervals with prominent horizontal lamination consist of claystone, siltstone, and shale (Figs. 8a, g), green to grey in colour. This LF is the most predominant fine-grained facies in the measured succession (Fig. 4b) and usually is associated with horizontally laminated (Sh), rippled cross-bedded (Sr) sandstone, coal (C), and massive mudrock (Fm) lithofacies with thickness from 0.5 m to more than 30 m. Some intervals include plant fossils (Fig. 8a). Laminated mudrocks usually have a gradual contact at the top and base (Figs. 8g, f).

The suspension-deposited lamina in fine-grained sediments suggest slow deposition in quiet water environments, where bioturbation was not intense enough to destroy the lamination. These facies have been deposited from suspension under a low water flow regime (Wright 1985; Miall 2000, 2006) and are interpreted as representing deposition in various environments from delta plain to marine offshore in the studied area.

Massive mudrock lithofacies (Fm)

This LF usually is accompanied by C and horizontally laminated mudrock (Fl) lithofacies (Fig. 8h) with dark grey to green colour. Its thickness is 0.5 to 10 m, with a gradual contact at the base, whereas the upper contact is usually sharply truncated. The massive appearance is due to the absence of fluid flow or gravity flow due to the deposition of material from suspension (Miall 2006). Fürsich et al. (2005) argue that this structure-less LF suggests a prevalence of low energy conditions and probable deposition in a protected coastal setting in the studied area.

Coal lithofacies (C)

This LF is most frequent at the base and less abundant in the upper part of the studied section; it includes less than 2% of the total succession (Figs. 4b, 7). The thickness of

coal seams reaches up to 3 m. These seams typically show gradual contacts at the base and sharp contacts at the top. Sharp contacts may indicate the removal of a part of the peat precursor material during switching channel or torrential crevasse flooding of the peats (Fig. 9e). In contrast, gradational contacts at the base of coal seams usually indicate a continuum of deposition and genetic relationship between the sedimentary and coal facies (Dai et al. 2020). Although the E coal seam, C1 is the thickest and has the most continuity in the area. The ash content is highest in the B2 and E coal seams and have the most partings (up to 5) among the other seams in the Parvadeh Area.

Many plant fossils (fragments and entire leaves) occur on the surface of coal layers (Fig. 8b). Coals are usually laminated, shiny with clarain lithotypes, and interlayered with rich organic partings of Fl and Fm lithofacies. These partings may be caused by fluvial channel filling contemporaneous with peat accumulation, tectonic activities, and fault actions. This LF was deposited in the studied area's vegetated swamps on delta/coastal plains.

In the Parvadeh coals, sulfur content is usually more than 1%, especially pyrite (Shariat Nia et al., 1997; Ahmadi, 2015; Zamansani et al., 2019). The B1 and D coal seams have most, and the E coal seam has less sulfur content (Shariat Nia et al. 1997). Pyrite is finely dispersed as framboidal and single crystals or fracture and pore filling. The sulfur content of coal is commonly influenced by the degree of seawater inflow during and after peat accumulation, especially during sea level rise (Vassilev and Vassiliva 1996; Chou 2012; Stock et al. 2016). In high-sulfur coals, seawater sulfate diffuses into the peat, where anaerobic sulfate-reducing bacteria reduce it. Reactions of the reduced sulfur species in interstitial water with iron and organic matter led to the formation of the mineral sulfides (mainly pyrite) and organic sulfur compounds (Vassilev and Vassiliva 1996; Chou 2012).

Medium-grained lithofacies

About 17% of the studied section comprises very fine to medium-grained sandstone (Fig. 4b), which becomes more abundant towards the top of the section. These layers have different sedimentary structures and geometries and are subdivided into five LF as below.

Horizontally laminated sandstone lithofacies (Sh)

This LF is common in the measured section and ranges from millimeters to 2 m in thickness with little fragments of coal and plant fossils. It consists of very fine to fine-grained sandstone and litharenite to sublitharenite petrofacies. The grains are well sorted and rounded, usually alternating with rippled cross-bedded (Sr) and planar cross-bedded (Sp) sandstone (Figs. 8e, g); these facies laterally changes to other sandstone
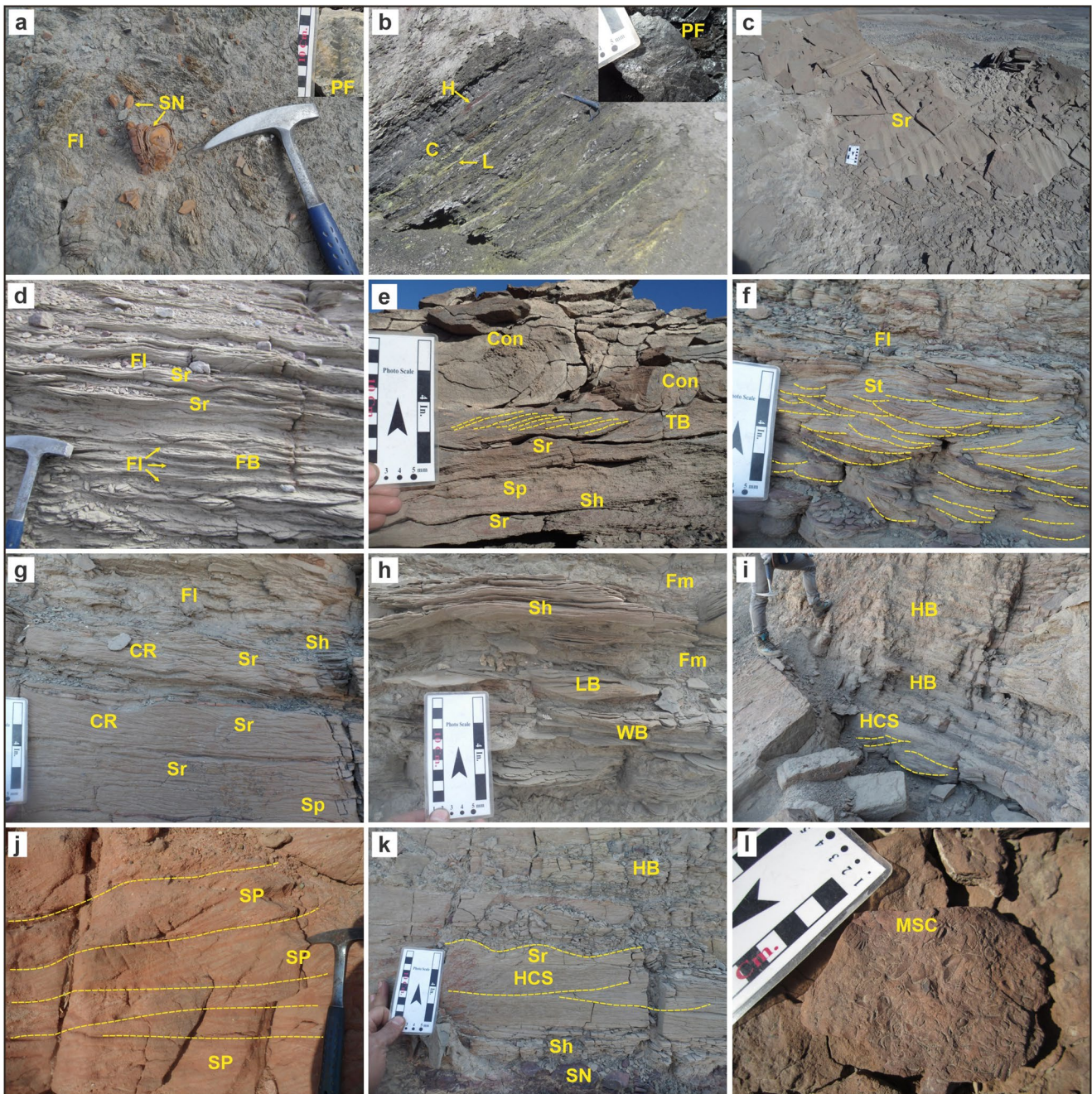
Fig. 8 Field photographs representative of different lithofacies (*LF*) identified along the Qadir member in Parvadeh section, **a** Horizontally laminated carbonaceous shale (*Fl*) with siderite nodules (*SN*) and a close view of plant leaf fossil (*PF*) on the upper right, **b** Parallel planar layers of coal LF (*B2* coal seam) with oxidized pyrite as limonite (*L*) and hematite (*H*) interlayers. Notice close view of PF on the upper right (*PF*), **c** Ripple cross-laminated sandstone LF (*Sr*) with oscillation-rippled surface, **d** Alternation of Sr Fl as flaser bedding (*FB*), **e** Co-occurrence of planar bedding (*Sh*), planar cross-bedded (*Sp*) and current Sr lithofacies which is capped with sigmoidal laminated tidal bundle (*TB*) marked by yellow dash line. Convolute structure (*Con*) overlying the TB, **f** the intersecting sets of red small-scale trough cross beds (*St*, yellow dash line) in fine bedded channel sand-stones overlain by Fl, **g** Sr with climbing current-rippled beds (*CR*). Aggradational ripples covered by Fl and Sh, **h** Heterolithic bedding (*HB*) association consists of lenticular (*LB*) and wavy-bedding (*WB*) which is overlain with alternation of Fm and Sh. **i** Hummocky storm cross-stratification (*HCS*) at the base and HB association of parallel-laminated, sharp-based sandstone, siltstone and mudstone, **j** Multiple sets of Sp with red colour resulting from oxidizing condition, **k** Co-sets of medium-grained LF which imply a shoreface environment, Sh, HCS with the erosional surface between underlying truncated lamina and overlying draped lamina, oscillation of Sr and HB at the top, **l** Sandy coarse-grained bioclastic LF (*MSC*) with bivalve, gastropod, brachiopod and echinoderm clasts with orange colour implying oxidizing condition in the shoreface environment
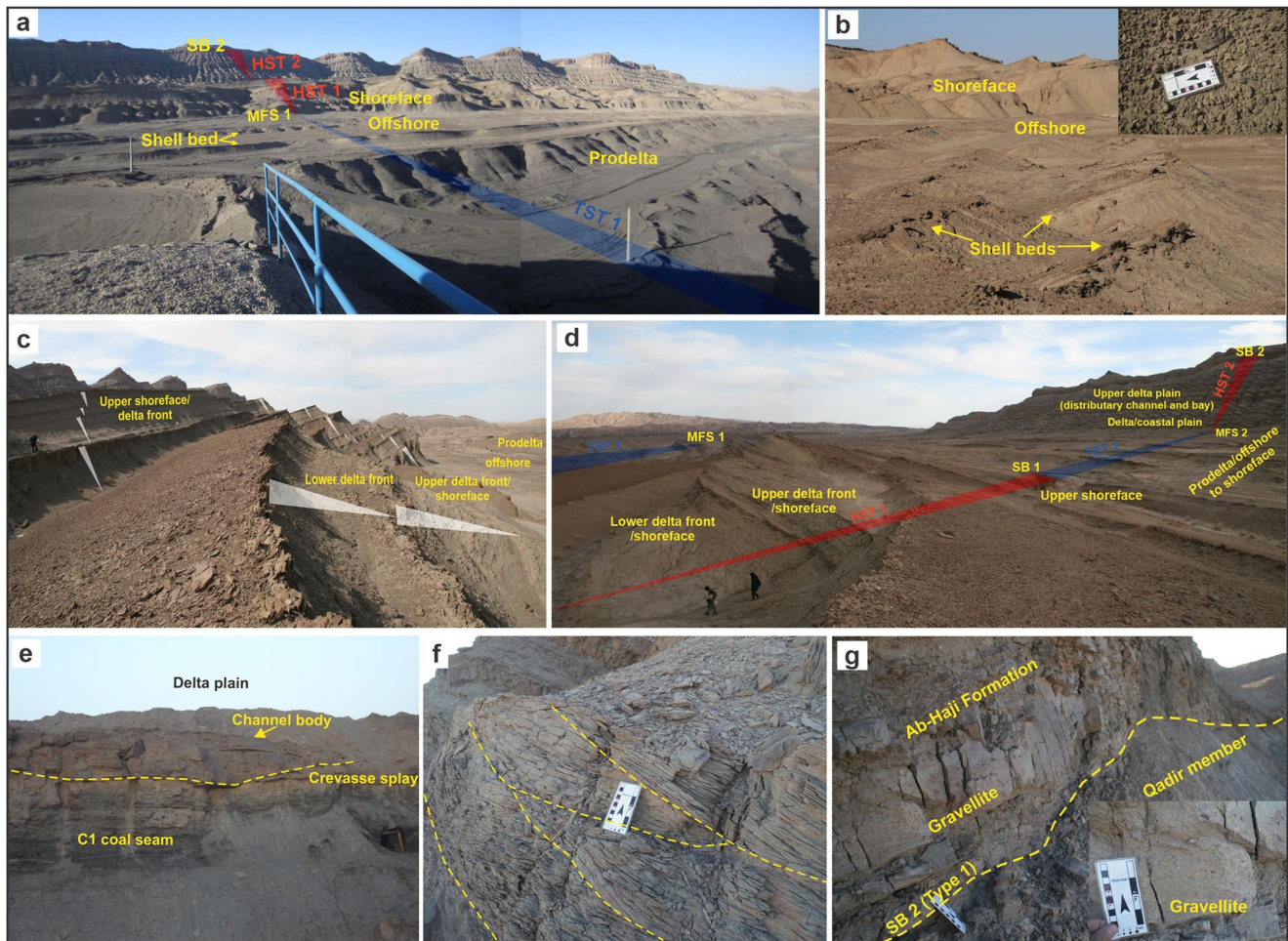
Fig. 9 Overview field photographs of facies associations (*FA*) and depositional sequences of the Qadir member, **a** Panoramic distance shot of first 3rd-order sequence composed of prodelta-offshore finning-upward cycle (*TST1*) and coarsening and thickening upward cycles of shorefaces FA (*HST1*), view toward the west-northwest. **b** Aggradational systems tract in the MFS1 includes sets of fine-grained offshore FA alternated with shell beds. Notice close view of shell bed (bivalve) and pavement structure on the upper right. **c** Thick stacking parasequence of delta front/shoreface FA at the HST1, view to the northwest. **d** Panorama field aspects of two 3rd-order T-R sequences of the deltaic-shallow marine systems, view to the southeast-east. **e** yellow dash line marks lower erosive flat to concave up base of channel fills directly overlying laterally continuous coal seam in the delta plain FA. **f** Close view of multiple stacked planar and trough cross bed from channel and mouth bars with lateral offset. **g** Sharp contact between Qadir member and Ab-Haji formation with micro-conglomerate horizon over a type 1 SB. Notice closeup view gravellite bed on the lower right

LF or mud rocks (Fl). Planar-stratified sandstones are commonly deposited within upper to lower flow regimes from unidirectional currents and traction transport mechanisms (Boggs 2009).

Rippled cross-laminated sandstone lithofacies (Sr)

This LF consists of current and wave-rippled, cross-laminated sandstone and is associated with the horizontally laminated and planar cross-bedded sandstome and horizontally laminated mudrock (Fl) lithofacies (Figs. 8d, e, g). The petrofacies

of this LF are sublitharenite to chertarenite with well sorted and rounded grains. Ripples occur due to subaqueous traction transport of granular materials under unidirectional currents or oscillatory low flow regime, as commonly observed for sand and silt size sediments (Figs. 8c, g).

The current ripples are commonly formed in crevasse splays/siliciclastic shallow marine environments, whereas the symmetrical ripples are often formed under wave effect conditions on a shallow marine siliciclastic shelf (Harm et al. 1975; Davis 2012). Ripples apices are usually straight, sinuous, and rarely linguidal. Overall, the presence

of current and wavy ripple marks in the studied section indicates a paralic sedimentary environment. The climbing ripple cross-lamination indicates gradually increasing flow speed and large amounts of sand (Fig. 8g), commonly caused by sedimentation in two limbs of the ripple marks (Harm et al. 1975; Miall 2006). Also, tidal bundle structure and sigmoidal cross-lamination (Fig. 8e) are indications of tide-storm interactions and are visible in delta and coastal plain settings.

Planar cross-bedded sandstone lithofacies (Sp)

This LF is the most abundant sandstone facies (Fig. 4b) and is visible, especially in the middle and top part of the sequence (Fig. 7). It comprises very fine to medium-grained sandstones with sublitharenite petrofacies. The grains are moderately to well-sorted and sub-mature to mature. These cross-bed layers usually have a low angle (5° to 15°) and are tabular and wedge-shaped (Figs. 8e, j). This LF alternates with Sh, Sr, and trough cross-bedded (St) sandstone. Rarely, herringbone structure is visible in this succession (Fig. 7), which indicates changes in flow direction and indicates a tidal environment.

This LF was deposited by migration of two-dimensional ripple marks and dunes with straight crests in response to a unidirectional current in the low flow regime, mainly close to river banks (distributary rivers here), intertidal zones, or lower shoreface (Davis 2012).

Trough cross-bedded sandstone lithofacies (St)

This LF is dominant at the top of the section (Fig. 7) with well-sorted and medium to well-rounded sandstone. This facies is intercalated by horizontally laminated and Rippled cross-laminated sandstones and Fl (Fig. 8f) and has low angle layers (5° to 15°).

Trough cross-bedding originates from the migration of three-dimensional bed forms, either small current ripples that produce small-scale cross-bed sets or large-scale ripples (dunes) (Boggs 2009). Trough cross-bedded facies were formed by sedimentation from unidirectional currents on linguoidal, sinuous or lunate ripple marks. They commonly accumulate under the turbulent flow regime of channel filling (Tucker 2001; Miall 2006).

Hummocky cross-bedded sandstone lithofacies (HCS)

This lithofacies is rare in the studied section and accompanied by Sh and Sr (Figs. 4b, 8i, k) at the upper and middle part of the succession (Fig. 7). These facies consists of very fine to fine-grained sandstone and siltstone and contains well sorted and rounded grains.

It seems that HCS originates from a combination of uni-directional and oscillatory flows related to wave and storm activity; it is generally regarded to be a fairly reliable indicator of deposition in shelf and shoreface environments (Boggs 2009). Tucker (2001) believes that this LF forms between fair-weather wave-base (FWWB) and storm wave-base (SWB), and if it is formed by the interaction of the coastal flow and storm, it could be accompanied by climbing ripple marks.

Heterolithic bedding lithofacies (HB)

This LF alternates with massive mudrock (Fl), Sr, and Sh and sometimes Fm and C (Figs. 8i, k); it indicates energy fluctuations in the sedimentary environment. The lithology of this LF is shale, siltstone, and sublitharenite sandstone; it is abundant in the middle and upper parts of the studied section (Fig. 7). Three main types of heterolithic bedding, i.e. flaser, wavy and lenticular bedding are visible in this LF (Figs. 8d, h). In the studied section, this LF is common in delta/coastal plain and subtidal origin deposits.

Mixed siliciclastic-carbonate lithofacies (MSC)

The petrofacies of this LF are sandy rudstone, sandy float-stone, and bioclastic sandstone. The thickness of these facies is from 5 cm to 2.5 m, and it is visible above coal layers in the middle part of the studied section (Fig. 7). These facies usually have an orange to red colour and pinch out laterally. The reddish colour of this LF is created by ferric oxides, notably hematite, and represents oxidizing environments. The fauna includes coarse fragments of echinoderms, gastropods, solitary corals, brachiopods, and bivalves (Figs. 5j-l; 7l), sometimes with micritic rims; when bivalves are more prevalent on the bed surface, a pavement structure forms (Fig. 9b).

The fine-grained sand and silt-size quartz with medium to good sorting and roundness, the large size of fossil debris, and negligible amounts of the micritic matrix indicate that the facies was formed in a relatively high-energy upper shoreface to offshore transition environment. Bioclastic or fossiliferous sandstones may be related to delta front to prodelta environments.

Facies association analysis

Six major facies associations (FA) were identified, which belong to deltaic and shallow marine siliciclastic depositional systems, representing delta/coastal plain, delta front, prodelta, and upper shoreface, lower shoreface, and offshore environments (Figs. 9 and 10).

Facies associations of the deltaic depositional system

Delta/Coastal plain facies association

Description: This FA is composed of thick fine-grained massive and laminated mudstones and shales (Fl and Fm), interbedded with coal seams (up to 3 m) with ferruginous concretions and rarely St lithofacies (Fig. 7). The main features of this FA include the presence of coal layers, plant fossils and overall abundant organic matter (Figs. 8a, b; 9g, h). Coal beds are usually continuous laterally, have lamination and show iron oxide and gypsum between their laminae, which indicates pyrite oxidation in outcrops (Figs. 8b, 10).

The thickness of this facies association varies from 15 to 60 m; it occurs at the base of coarsening upward cycles that are often topped by thin sandstones with marine fossils and/ or trace fossils (Fig. 7). Sp, Sh, and Sr (wave and current ripple marks) sandstones show sheet-like geometry, usually with calcite, iron oxide and siderite cement in some horizons (Fig. 7) and have sporadic *Arenicolites*, *Lockeia*, *Bergaueria*, *Planolites*, *Thalassinoides* and *Teichichnus* trace fossils (Figs. 7, 11, 12).

Channels in delta plain facies are characterised by 1-2 m sandstone bodies with lower sharp, erosive, concave to flat boundaries with a subtle upward-finning trend (Fig. 9e). They change to heterolithic deposits, often with asymmetrical ripples, particularly in their upper parts. The main structures of channel-fills are multi-tabular layers around 5-20 cm thick with dominant trough cross-bedding and sub-parallel beds in between (Fig. 9f). The channel sand bodies commonly contain plants and coal fragments and typically display no or very limited bioturbation in the lowermost part. This is typical of channels on delta plains (Li et al. 2011; Bayet-Goll and Neto De Carvalho 2017; Anell et al. 2021). These channels have lateral offset stacks (Fig. 9f), especially at the top of the Qadir member.

Interpretation: The abundance of fine-grained sediments in this kind of FA indicates sedimentation in low energy conditions from suspension in the interdistributaries (Bhattacharya 2006) and sandstones registering the increasing energy of the shallow water as the bay fills with crevasse splay sediment (Thomas 2002). This FA's dark and pale green colours indicate a reducing condition (Miall 2000). Waves and tides may cause complete reorganisation of deltaic deposits (channel, distributary mouth bar, and interdistributary facies) in the lower delta plain to form shoreline to shallow marine affected sand as in the lower part of the section. In contrast, upper delta plain sediments remain largely unmodified, except through later erosion by channels, such as at the top of the Qadir section (Wright 1985; Elliott 1986; Fielding 1987; Bhattacharya 2006; Dai et al. 2020).

The delta plain was incised by sand rich, straighter and narrower fluvial distributary channels. Anell et al. (2021)

belive that the wave and storm likely confining coarser deposits up-river in these environments. This probably is the reson of the absence of coarse-grained LF in the Qadir sedimentary system. The presence of hummocky cross-bedded sandstone (HCS), wavy Sr, tidal bundles, and marine ichnofossils imply the effects of marine phenomena (e.g. wave and storm) on the channel sediments. Sandstones in the mouth bar at the end of distributary channels usually show a coarsening-upward trend, relatively thick Sp, St, Sh lithofacies, wave, current and climbing ripples (Sr) and thin Fl containing plant debris (Fig. 9f). The point bars are commonly characterised by HB resulting from changes in the hydraulic regime (Fig. 8i). The trace fossil suits in the delta plain commonly are attributed to *Skolithos* ichnofacies (MacEachern and Gingras 2007), possibly controlled by low salinity, high-energy and/or episodic sedimentation (Bayet-Goll and Neto De Carvalho 2017).

Distributary channels are wider and fewer in the lower part of the Qadir studied section, and coals are generally relatively thin and widespread (Fig. 7e). Usually, wave-influenced deltas are fed by fewer distributaries than river-influenced deltas (Bhattacharya 2006), like at the base of the section (Fig. 7).

Unlike the lower coal seams, seemingly upper ones in the Qadir member (E coal seams) were formed in the upper delta plain. These swamps developed in sediment-infilled interdistributary areas, and aggradation and erosion were controlled by lateral and seaward migration of the channels, point-bar accretion, and levee-breach crevassing into interdistributary bays (Bhattacharya 2006; Dai et al. 2020). Linear, lenticular sandstone bodies dominate these deposits, and the thin corresponding E coal seam is limited in lateral extent (Shariat Nia 1997).

Between the upper and lower delta plains, a transition zone was exhibited. This zone consists of a widespread platform on which peat mires are formed with thicker and more widespread coals than on the lower delta plain (Fielding 1987; Scott 1989). According to facies successions, it appears that this transitional environment corresponds to the thicker C1 coal seam.

Delta front facies association

Description: This FA commonly is characterised by coarsening and thickening upward successions. The sediments are partly interbedded with deformed sandstones and lenses with convolute bedding and internal folding. Convolute bedding is usually pinched out and truncated by the upper bedding surface, showing a flat top. Cross-stratified sandstone strata are locally arranged in tidal bundles (Fig. 8e). Thickness of sandstones is up to 2 m, interlayered between shale, mudstone, and silty shale.

Most of the layers have no trace fossils and a low bioturbation index. However, some trace fossils, such as *Skolithos*, *Thalassinoides*, *Planolites*, *Rosselia, Bergaueria*, *Arenicolites*,
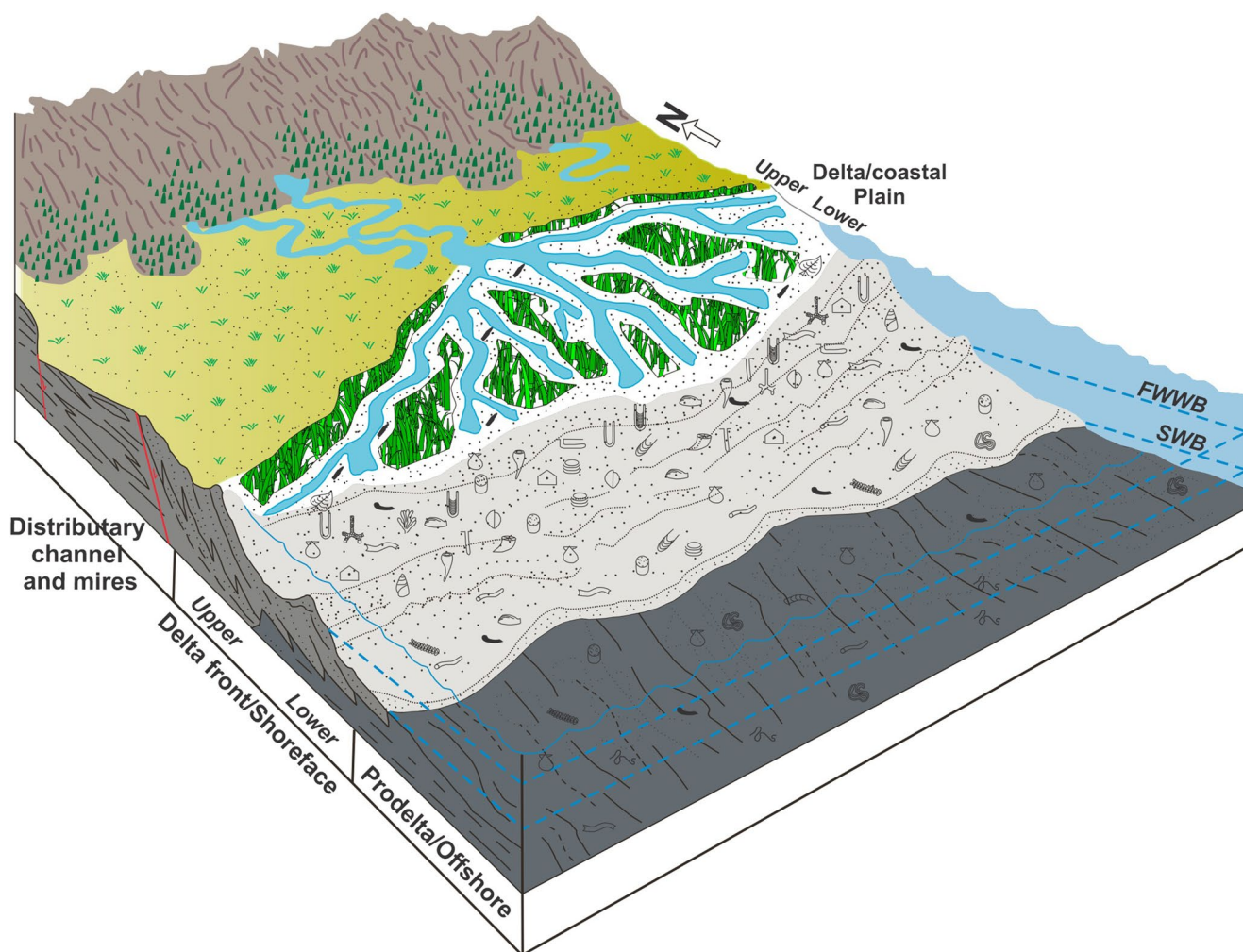
Fig. 10 Schematic sedimentary environment model of Qadir member in the Parvadeh Area showing paralic system sediments: a progradational delta dumps sediments onto a shallow marine siliciclastic shelf (modified from Bayet-Goll and Neto De Carvalho 2017). Legend of the symbols is given in figure 7

and *Lockeia,* are scattered in some sandstone horizons (Figs. 10, 11), most of them belonging to suspension and deposit feeder organisms (Bann et al. 2004). These horizons usually have sporadic shell fragments.

Interpretation: The sediments derived from the delta front environment are usually reworked, reshaped, or removed by basinal processes. Soft sediment deformation is interpreted as gravity-driven mass flow, sediment failures and/or seismities (Bhattacharya 2006; MacEachern and Gingras 2007). Convolute bedding structures and possible slumped beds are related to the high sedimentation rate and supply over a small-scale steep topography. Also, climbing ripples near mouth bars suggest rapid sediment input. The presence of cross-bedding, bidirectional cross-strata, rhythmic lamination and bundling, and symmetrical ripples may indicate that the system was at least locally impacted by waves and tidal currents along the delta front (Anell et al. 2021) (Fig. 7).

Fine-grained lower delta front sediments are more abundant in the upper part of the section comprising interbedded dark to grey shale and silt with thin and regular interlayers of sandstones. The occurrence of HCS places these deposits above SWB as a result of storm-induced oscillatory currents or instability events (Bhattacharya 2006).

Delta front deposits at the base of the succession show low bioturbation intensities, though diversities are moderately high (Fig. 7). Delta front settings in the studied section have mixed *Skolithos* and *Cruziana* ichnofacies. However, in the upper delta front, *Skolithos* ichnofacies is more prevalent.

Prodelta facies association

Description: This FA consists of high volumes of fine-grained, structureless LF with laminated marine mudstone, fissile shale (Fl and less Fm), and intercalations of Sh and
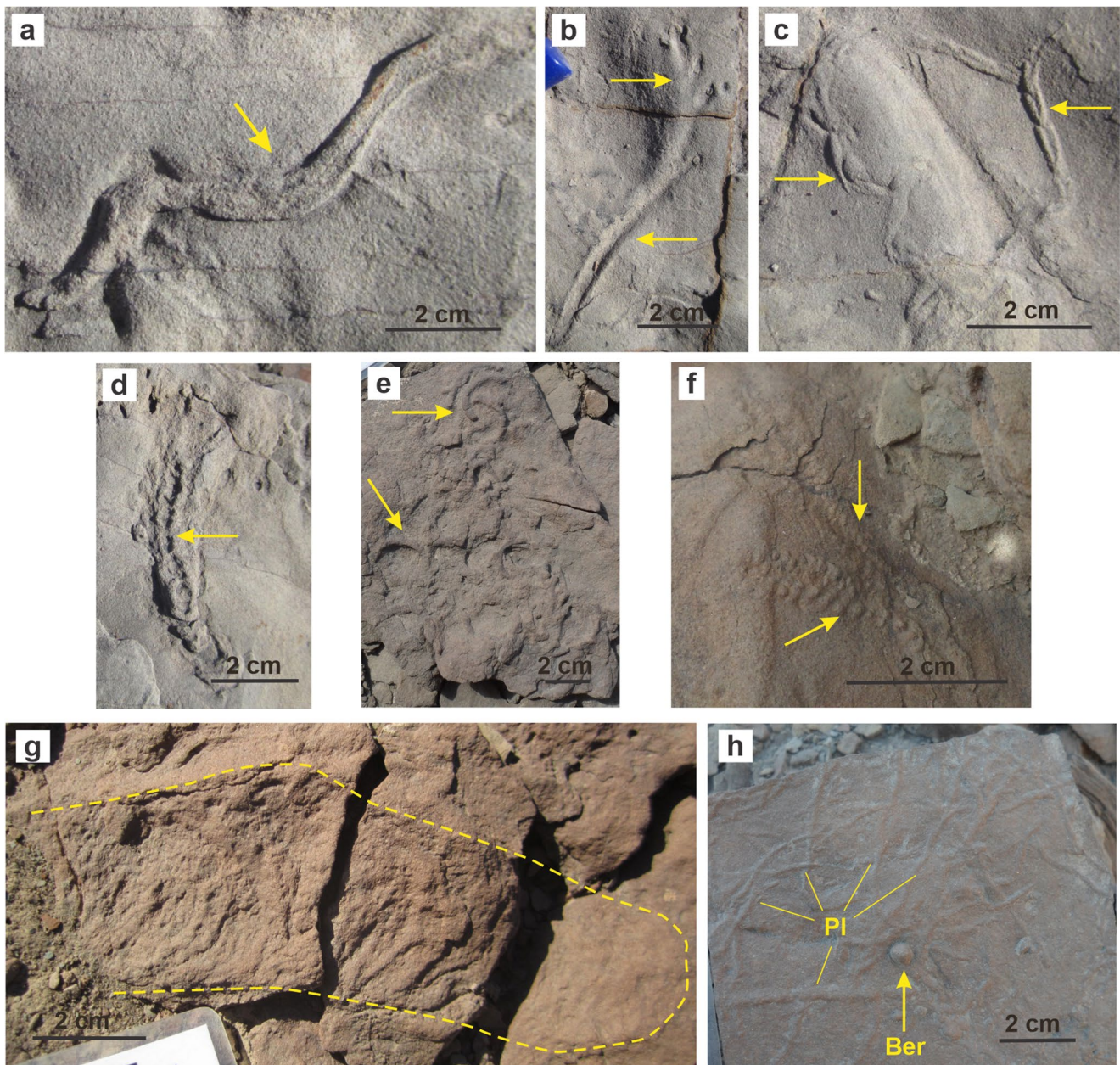
Fig. 11 Outcrop photograph of ichnogenera of the Qadir member, **a** *Helminthopsis abeli*, **b** *Phycodes*, **c** *Gyrochorte comosa*, **d** *Taenidium barreti*, **e** *Scolicia*, **f** *Protovirgularia*, **g** *Rhizocorallium jenense*, **h** *Planolites* (*Pl*) and *Bergaueria* (*Ber*)

Sp. This FA contains plant debris, considerable organic matter in some horizons, and occasionally marine fossils (bivalves), which commonly are organised in normal (fining upward) and rarely reverse (coarsening upward) sequences and grade into overlying open marine (offshore) FA with more fossils at the top (Figs. 7, 9a, 9c).

These facies display low bioturbation and limited trace fossils with low diversity, such as *Taenidium, Helminthopsis, Phycodes*, and *Gyrochorte* trace fossils (Figs. 11, 12),

which as *Cruziana* ichnofacies represent stable, low-energy environmental conditions (Bann et al. 2004; MacEachern and Gingras 2007).

Interpretation: This FA was deposited below SWB, with no structures related to wave and storm phenomena. Based on their lithology and close association with delta front sediments (Fig. 9a), they are interpreted as a prodelta setting with low to intermediate energy (Wright 1985). The sandstone, siltstone, and shale alternations record deposition by
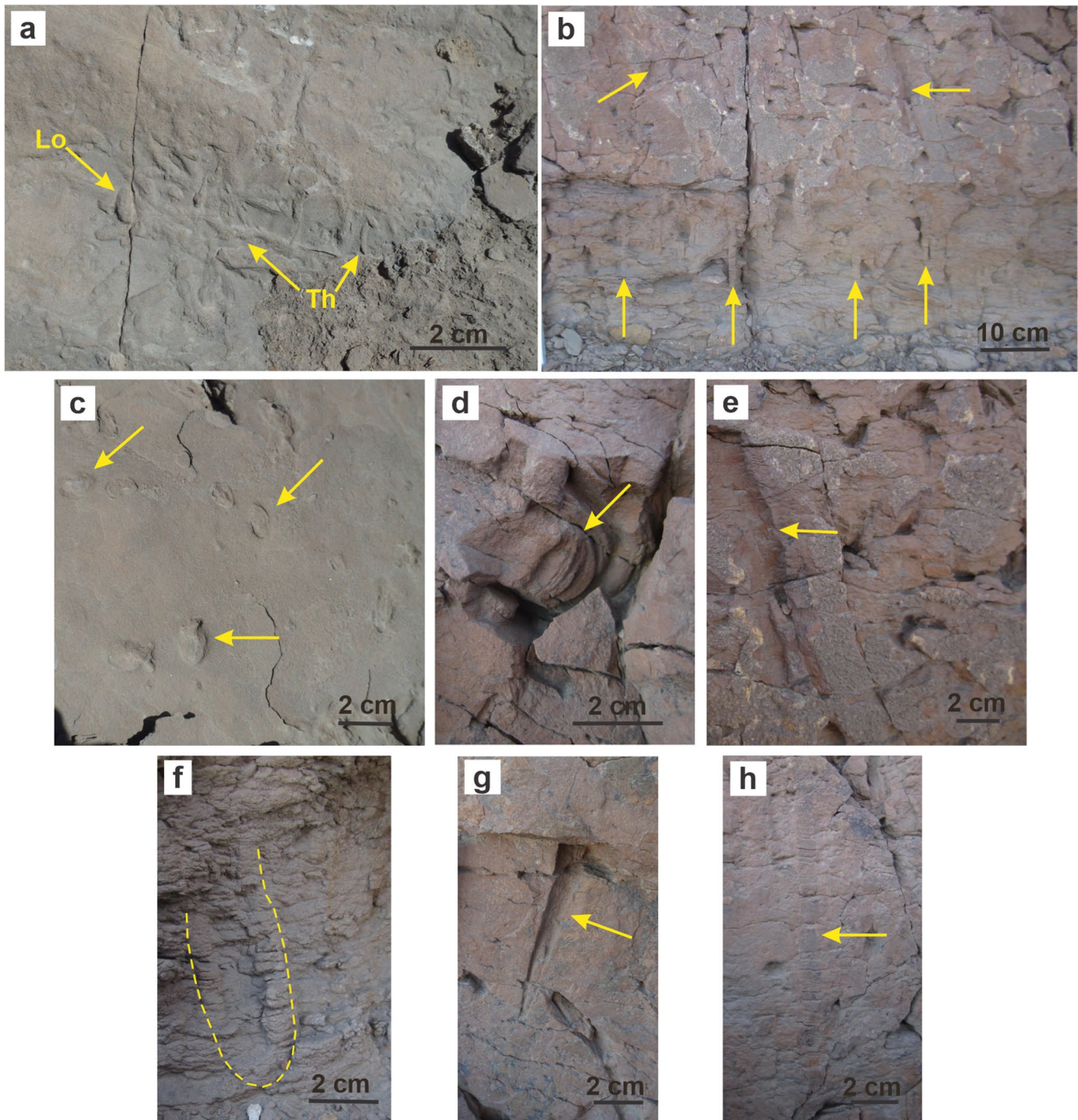
Fig. 12 Outcrop photograph of ichnogenera of the Qadir member, **a** *Thalassinoides* (*Th*) and *Lockeia* (*Lo*), **b** Intensive bioturbation as a pipe-rock ichnofabric in the upper shoreface (*arrows*) suggests a suit attributable to *Skolithos* ichnofacies, **c** *Skolithos*, **d** *Diplocraterion*, **e** *Ophiomorpha*, **f** *Arenicolites*, **g** *Rosselia*, **h** *Teichichnus*

suspension and density currents and can be interpreted as prodelta hyperpycnal currents caused by turbidity currents.

Lamination and fine-grained LF abundance indicate low energy systems and rare trace fossils, high organic matter and pyrite content imply oxygen-depleted bottom water conditions. Many intervals include structureless mudstone, reflecting abundant deposition of fluid mud and soup ground conditions development.

Facies associations of shallow marine siliciclastic shelf depositional system

Offshore facies association

Description: This FA is composed mainly of laminated mudstone and fissile shale (Fl), grading upwards into sets of heterolithic LF with scattered sandstone lenses (Fig. 9a). These sandstone beds (5-10 cm) are characterised by Sh and Sr lithofacies, rarely with current ripples. Also, it shows sheet-like geometry, and some fine-grained horizons have considerable amounts of organic matter and pyrite crystals. Burrowing is limited and includes *Taenidium*, *Gyrochorte*, *Helminthopsis,* and *Scolicia* (Figs. 10, 11, 12).

This FA is visible in the middle of the studied section (Fig. 7). There are large body fossils of bivalves and brachiopods in some layers (Figs. 9a, b), which implies shallow parts of the shelf. Offshore units associated with non-deltaic shoreface intervals typically contain diverse *Cruziana* ichnofacies.

Interpretation: Similar to prodelta FA, this FA is formed beneath the SWB. These settings display a close affinity with prodelta units. Notwithstanding, based on lithological and sedimentological features and their close association with shoreface FA, this facies is interpreted as the offshore setting.

The lack of oscillation-driven deposits indicates an offshore setting beyond the effect of the waves (Bhattacharya, 2006). The presence of marine fossils, such as bivalves, corals, and brachiopods, also points to a quiet open marine setting (Fig. 9b). Low energy and reducing conditions in some horizons may be indicated by abundance of fine-grained LF, low bioturbation index, pyrite and siderite minerals. Li et al. (2011) believe that thin sandstone layers in this sedimentary environment are commonly deposited by turbulent currents supplying sands from the shoreface. Those may form by storm-related transportation of sand into deeper-water zones where mud deposition normally occurs.

Lower shoreface facies association

Description: In this setting, fine-grained sediments are more abundant (Fl) and interlayers of fine to very fine-grained sandstones (up to 0.5 m thickness) (Fig. 9c) with Sh, Sr, Sp, HCS, and heterolithic bedding (HB). Sandstone layers exhibit sheet-like geometry, and marine body fossils such as bivalves, gastropods, brachiopods, echinoderms, and solitary corals are locally concentrated (Fig. 8l). This FA is visible in the middle of the outcrop section (Fig. 7).

Sandstones are usually topped by ripple surfaces and have a relatively low bioturbation index containing *Skolithos*, *Diplocraterion*, *Rosselia*, *Arenicolites*, *Rhizocorallium*, *Thalassinoides*, *Protovirgularia*, *Paleophycus*, and *Planolites* (Figs. 10, 11, 12). This FA commonly shows coarsening and thickening-upward trends and is usually overlain by upper shoreface sediments (Figs. 9b, c).

Interpretation: This FA belongs to the part of the marine system located below FWWB and above SWB (Wright 1985). Low to moderated bioturbation, fine to medium-grained LFs, and mixed *Cruziana* and *Skolithos* ichnofacies point to a variable and fluctuating hydraulic energy in this environment (MacEachern and Gingras 2007).

Generally, a combination of horizontal lamination and oscillation ripple marks indicates deposition by waves. Also, hummocky and wave-ripple lamination are typical of storm deposits formed under the influence of combined flow and point to an environment affected primarily by waves rather than currents (Bann et al., 2004; Anell et al., 2021). The predominance of HCS indicates deposition below FWWB, where oscillatory flow, associated with storms, is the most common hydrodynamic mechanism. The planar lamination was formed in the upper flow regime during intensive wave activation. Lenticular and wavy bedding and extensive bioturbation indicate a lower energy environment than the upper shoreface and foreshore.

Upper shoreface facies association

Description: Pervasive, sheet-like sandstone with wavy and current Sr, low angle planar, and bifurcation Sp interlayered with thin mudstone and shale indicates variable hydraulic energy for this FA (Fig. 9c). This part of the sedimentary bed set exhibits bidirectional cross-bedding. Sandbeds show climbing ripple stratification, tidal bundles, and HCS and HB facies, which usually have red colour (Fig. 8d). This facies assemblage, along with lower shoreface facies, prevails in the middle part of the outcrop section (Fig. 7). Bivalves, brachiopods, gastropods, and echinoderms are common fossils. A variety of trace fossils is observable in this FA, such as *Ophiomorpha*, *Skolithos*, *Arenicolites*, *Rosselia*, *Planolites*, *Thalassinoides*, *Lockeia,* and unknown horizontal burrows (Figs. 9, 10).

Interpretation: This part of the sedimentary succession is located above FWWB and deposited in a high-energy regime, and the marine fossils imply average marine salinity (MacEachern and Gingras 2007). There is a variety of trace fossils, more than in the lower shoreface, and burrows are mainly attributable to the *Skolithos* ichnofacies in pipe rock ichnofabric (Fig. 12j) with cylindrical or U-shape regarded as an indicator of a high-energy environment. The occurrence of diverse and robust trace fossil suites suggests low sedimentation rates, sufficient nutrient supply, and oxygen near the bottom induced by the mixing of water by waves or currents and a relatively stable substrate (Li et al. 2011).

Storm sand layers show climbing ripple stratification and HB indicators of tidal and subtidal influences. In this FA, the strong wave influence may be suggested by the presence of wave ripples, short wave-length HCS, and shell gravel indicative of storm events acting in an open coast environment (Anell et al., 2021). The red colour of the sediments further indicates oxic bottom water conditions.

Due to marine effects on the deltaic environment, discrimination between deltaic, coastal, and shallow marine facies is difficult (Bann et al. 2004; MacEachern and Gingras 2007), but this study's ichnofacies analysis was efficient. Trace fossil studies of the Qadir succession in the Parvadeh area show *Skolithos*, *Cruziana*, and mixed *Skolithos-Cruziana* ichnofacies. The *Cruziana* ichnofacies is attributed to the distal delta front, prodelta, and offshore, whereas *Skolithos* ichnofacies are related to the delta plain and upper shoreface and the mixed *Cruziana-Skolithos* ichnofacies to the delta front and lower shoreface (Fig. 10). Also as a general rule, non-marine deposits contain fewer trace fossils than marine deposits and thick, rapidly deposited beds contain fewer traces than slowly deposited ones and high-energy facies, typically have little bioturbation (Bann et al. 2004; MacEachern and Gingras 2007). This rule was helpful to distinction between prodelta muds and offshore mud dominated systems.

According to this sedimentological investigation, the Qadir member is a succession representing a paralic system (Fig. 10). This deltaic setting was mostly river-dominated and influenced by marine events, especially by waves and storms. Some of the arguments for a river-dominated delta are common fine-grained LF, considerable thickness of delta plain FA, extended distributary channels, and soft sediment deformation caused by high sediment supply (Harms et al. 1975; Wright 1985; Bhattacharya 2006). Symmetrical and bifurcation structural features, prevalence of mouth bar sediments (particularly at the top of the section), heterolithic succession, hummocky structure, intercalation with shoreface sediments containing marine body and trace fossils, sandstones with textural maturity, medium to well sorting and roundness prove the effects of wave and storm activity within the deltaic system. The lack of conglomerates in this succession is possibly due to wave effects or the long distance of the paralic environment from the sedimentary sources in the hinterland.

The sheet-like distribution and the maturity of the sandstones, as well as the lack of elongated sandstone bodies, suggest rapidly shifting active delta lobes along a shoreline. Seaward progradation and aggradation of river-dominated deltas commonly are the modes of delta plain construction, assisted by a great number of ephemeral terminal distributary channels that form mouth bars; these delta plains coalesce to form a large delta lobe, which is occupied by wetlands with a high potential of forming swampy freshwater mires (Bhattacharya 2006), like in the Parvadeh Area.

FA analysis shows that peatlands were formed and extended on the delta plain environment, which was influenced by marine water. It seems that the coal-bearing interval at the base of the section belongs to the lower delta plain to the transitional environment to the upper with insubstantial distributary channel-fill deposits; coals are thin to medium thick and widespread. The peats associated with lower delta plain settings tend to be planar, often split, and with high ash and sulfur contents (Scott 1989). Seemingly, the upper coal layers formed on the upper delta plain (E coal seam). This part of the delta plain is highly influenced by distributary channels, crevasse channels, and splays with locally thicker and discontinuous coal seams, which tend to have lower sulfur and ash contents.

Sequence stratigraphy

Two large-scale depositional sequences (3rd order?) have been identified in the studied section (Seq. 1 and Seq. 2), which correlate with the Haq (2018) global sea level changes on short and long terms (Fig. 7). In short terms scale, it seems that the studied interval is equal to tow last sequences of the Upper Triassic with the age of about 4 million years. These depositional sequences are composed of transgressive systems tract (TST), maximum flooding surface (MFS) and highstand systems tract (HST), whereby the transgressive mainly consist of deepening upward trends, and regressive contain shallowing upward FAs (Figs. 7, 8e). These systems tracts are confined between two MFS (MFS1 and MFS2) and two sequence boundaries (SB1 and SB2, Fig. 7). Each sequence consists of several fourth-order sequences containing various smaller fining and coarsening upward parasequences. The base of Seq. 1 is covered by mining activities or does not have an outcrop. The systems tracts consist of numerous parasequences that are well developed and range in thickness from less than 2 to about 40 m, with most settings being less than 10 m thick (Fig. 7). These differences in sequence thickness reveal the influence of the additional factors as well as eustatic sea level changes, i.e. tectonic events and maybe climate fluctuations (Fürsich et al. 2005). The cycles thicker than about 20 m are usually caused by allocyclic mechanisms like tectonic activity, changes in eustatic sea level, and sediment supply (Miall, 2000), but smaller ones might be related to distributary channel migration, flooding, and crevassing, as it is visible along the surface section (Fig. 9e)

Rare thin intervals of carbonate sediments and sandstones with brackish marine fauna and *Cruziana* ichnofacies indicate a strong marine influence connected to a rise in relative sea level. These layers overlie the coal-bearing FA at the base of the section and are near the lower 3rd order MFS. Shiers et al. (2017) suggested that post-depositional

autocompaction of the mires resulted in marine incursion over broad areas of coastal /delta plain environments and could increase the effects of marine on these environments during TST. These abundant shallow marine fossils support a tropical climate and warm marine water at the end of the Triassic at a palaeolatitude of 25-35° N for the Tabas Area (Nützel and Senowbari-Daryan 1999; Seyed-Emami 2003; Wilmsen et al. 2009a). The sharp erosional surface at the top of the studied setting (SB type 1, Fig. 9g), and the end of the overall coarsening/shallowing upward cycles serve to identity the SBs (Fig. 7; Figs. 9a, d, g).

Parasequence boundaries of TST1 are marked by delta plain/shoreface sandstones at the tops of coal seams and carbonaceous mudstones. This succession pattern is repeated in TST2 but without any coal seams. Sediments with marine dinoflagellate cysts (Sabbaghiyan et al. 2020) in Parvadeh usually overlie the coal seams in Seq. 1 and show more marine influence in this sequence. A sandy substrate assemblage below FWWB is widely distributed and commonly occurs at the base of thickening upward cycles, primarily red-coloured, bioturbated, and shell-rich sandstones. In most cases, this assemblage characterises parasequences of the TST and early HST. It is indicative of lower shoreface to offshore environments (Fig. 9a). Several distinct types of coarsening and thickening upward cycles in the HST1 are produced by coastal/delta regression and progradation (lateral accretion), where there is a gradation from low energy offshore to high energy onshore facies (Fig. 9d).

In fluvial-dominated deltas like those in HST2, considerable numbers of shallow, narrow, and ephemeral terminal distributary channels can form intimately associated with mouth bars that form larger depositional lobes (Fig. 9f). As deltas prograde, these settings are recorded by upward coarsening and thickening sediments. Late HST2 is characterised by a strongly progradational upper delta plain facies assemblage that overlie muddy deeper water prodelta facies (Fig. 7).

The overall shallowing upward succession and pattern of increasing distributary channel sediments with thicker sandstone layers and more lithic grains and micritic matrix show that the top of Nayband Formation (Qadir member) is robustly progradational and indicate tectonic uplift reactivation of source areas. This pattern was observed not only on a regional but also on a basin-wide scale (Vassilev 1984; Fürsich et al. 2005; Wilmsen et al. 2009b; Salehi et al. 2015; Zamaniyan et al. 2018; Krystyn et al. 2019; Etesampour et al. 2020). Therefore, despite a favourable humid-temperate climate, few peat mires/coal seams were formed in the deltaic environment at the base of HST2, and coals are absent at the top of the sequence (Fig. 7). During sedimentation of this succession, lowered sea level drew down the coastal aquifer and lowered the groundwater table. The net effect of a sea level fall commonly diminishes the accommodation space

for mires and thus the likelihood of accumulating thick peat deposits (Bohacs and Suter 1997). Also, a change in subsidence pattern increased sedimentary supply was probably related to tectonic activity of the area and may have resulted in limited space for peat mires at the end of this depositional stage. In this condition, no continuous peat accumulates due to falling or low groundwater table, sedimentary bypass, and extensive erosion by fluvial channels (Bohacs and Suter 1997).

Accommodation is commonly a function of subsidence and base level. For mires, the base level is very specially the groundwater table. The base level in a paralic setting, such as in the studied succession, is believed to be the groundwater table, which is strongly controlled by sea level and hydrologically connected to the sea in near coastal paralic settings. If the sea level rises, its effect can extend more than 40 km inland (Filint et al. 1995; Banerjee et al. 1996; Bohacs and Suter 1997). The sequential position of coal seams related to changes in the types and trends of surrounding sediments shows that they are restricted to TST1 and early HST2 (Fig. 7). In this succession, the thickest (moderately thick) and most extensive coal layers fall dominantly into the TST (C coal seam). Coal-bearing intervals usually coincide with aggradational to slightly retrogradation stacking patterns, and in these conditions, ratios of subsidence over peat production are balanced for the longest time (McCabe 1993; Flint et al. 1995; Bohacs and Suter 1997). Also, in these parts of systems tracts, the clastic influx was more limited. According to the Bohacs and Suter (1997) model, in order to achieve such thick peat accumulation, accommodation space has to be created at a rate that approximately balances with peat growth period. The composite E coal seam at the top of the section is located in early HST2 (aggradational parasequence) and is thinner and more discontinuous than the lower coal seams, which are located at the base of the setting. Some discrepancies between coal seam thickness and continuity patterns in the Parvadeh coal seams, as predicted by the Bohacs and Suter (1997) model, may be due to local base level/sea level changes, subsidence rate, and/or sediment supply.

According to Bohacs and Suter (1997) model, in order to considerable peat accumulation, accommodation has to be created at a rate that approximately balances with peat production or slightly exceed the peat accumulation rates, with the ratio of accommodation rate to peat production rate being 1-1.18. If the rate of accommodation creation outstrips peat production, the mire is drowned and inundated with the sediments. Conversely, if peat production exceeds the rate of accommodation creation, the mire is exposed, oxidized, and reworked. Almost all of the coal seams in the Parvadeh Area are composite and have one to more than three inorganic partings, i.e. clastic layers representing flooding of topogenic to transitional peat mires. This condition was caused by

increasing the accommodation rate to peat production rate to more than moderate, i.e. 1.18 (Bohacs and Suter 1997). The development of significant splitting of the Parvadeh coal seams indicates a generally unstable depositional environment, which is considered a function of the tectonic setting of this region, i.e. vicinity to the northern margin of the Neo-Tethys foreland basin, which is characterised by the faults active at that time such as those surrounding the studied area (e.g. Nayband and Kalmard faults). In these mires, the ash content of peat was high, and sediments were flooding the topogeneous mires from rivers (over bank deposits, crevasse splays) and the sea during storms or high tides.

The coal seams' thickness and quality vary between the region's eastern and western parts. Seam parting and coal ash content are more abundant in the west than in the east. The coals usually are categorized into medium to high ash coal with an average of 13 to 50 wt% ash, which is highest in the B2 seam and lowest in the D seam (Shariat Nia et al. 1997). According to previous studies, peat formation for each coal seam initially occurred in western parts and developed eastward towards the marginal marine environment. Therefore, coal seam thicknesses decrease eastward, and some even pinch out (Shariat Nia 1994; Shariat Nia et al. 1997).

Conclusions

Integrated sedimentological, ichnological, and sequence stratigraphic studies of the Qadir coal-bearing member in the Parvadeh Area provide essential clues to the depositional environment during the Late Triassic.

- Facies analysis of the Qadir outcrop section resulted in recognition of ten lithofacies and six facies associations related to delta/coastal plain, delta front, prodelta, lower and upper shoreface, and offshore settings. According to the sedimentological and sequence stratigraphic studies, the Qadir member is a succession of paralic system sediments; they represent a progradational delta that partly developed into a shallow marine siliciclastic shelf; thus, the deltaic setting was mostly river-dominated but temporarily influenced by marine conditions.
- The economic coal-bearing interval at the base of the section is attributed to peat deposition in mires in the lower delta plain or transition zone between the lower and upper delta plain. These coal seams tend to be planar with low to medium thickness, often with numerous partings and high ash and sulfur content.
- Two depositional sequences (maybe third order) are identified in the studied section, which correlate with global sea-level fluctuations. In the sequence stratigraphic

framework, the coal seams are restricted to the middle part of the TST1 and early HST2, which had higher rates of accommodation and limited clastic input, permitting the evolution of widespread peatlands. The main economic coal zone falls dominantly within the TST1.
- Water-born ash and partings indicate that the coal-forming environment was a low-lying, topogenous flow-fed area near detrital point sources with moderate to high accommodation to peat production ratios, the inability of vegetation type and density to baffle water-borne sediments and changes in acidity in conjunction with the influx of fresh or saline water. In addition, the development of significant splitting and high ash coals in the area indicates generally unstable conditions, which can be related to the tectonic setting of the Neo-Tethys foreland basin, which is likely characterised by contemporaneously active faults.
- The sediment stacking pattern of the Qadir member over the marine sediments of the Howze-Khan Member, clearly illustrates the advanced stage of the marine basin filling with limited accommodation space. The rate of subsidence and sediment supply was roughly at equilibrium so that no major environmental changes occurred. Toward the end of the Triassic, in connection with the general shallowing trend, open marine conditions (Howze-Khan Member deposits) were increasingly replaced by marginal marine, i.e. deltaic environments with coal formation (Qadir member). The opening and spreading of the Neo-Tethys, in the Rhaeto-Liassic time provided favourable conditions for high humidity at low latitudes, which caused lush vegetation.

According to the palaeoenvironmental reconstruction, the coal layers may be thicker, with less sulfur (pyrite) but more ash toward the western part of the Parvadeh Area. This sequence is concealed under the younger sediments due to differential subsidence in response to block tilting and faulting. These coal resources presently do not have economic value for mining but may be suitable as coal bed methane resources.

Declarations

Conflicts of interests The authors have no relevant financial or non-financial interests to disclose. The authors have no competing interests to declare that are relevant to the content of this article. All authors certify that they have no affiliations with or involvement in any organisation or entity with any financial interest or non-financial interest in the subject matter or materials discussed in this manuscript. The authors have no financial or proprietary interests in any material discussed in this article.

References

Ahmadi, A. (2015). Characterization and Washability of Pyrite in High, Sulphur Coals from Tabas, Iran. *Journal of Chemical Engineering and Chemistry Research 2*, 457-466.

Anell, I., Zuchuat, V., Röhnert, A. D., Smyrak-Sikora, A., Buckley, S., Lord, G., Maher, H., Midtkandal, I., Ogata, K., Olaussen, S., Osmundsen, P. T. & Braathen, A. (2021). Tidal amplification and along-strike process variability in a mixed-energy paralic system prograding onto a low accommodation shelf, Edgeøya, Svalbard. *International Association of Sedimentologists and European Association of Geoscientists and Engineers, John Wiley and Sons 33*, 478-512.

Banerjee, I., Kalkreuth, W. & Davies, E. H. (1996). Coal seam splits and transgressive-regressive coal couplets: a key to stratigraphy of high-frequency sequences. *Geology 24*, 1001-1004.

Bann, K. L., Fielding, C. R., MacEachern, J. A. & Tye, S. C. (2004). Differentiation of estuarine and offshore marine deposits using integrated ichnology and sedimentology: Permian Pebbley Beach Formation, Sydney Basin, Australia. In D. Mcilroy (Ed.), The Application of Ichnology to Paleoenvironmental and Stratigraphic Analysis. *Journal of Geological Society of London Special Publication 228,* 179-211.

Bayet-Goll, A. & Neto De Carvalho, C. (2017). Differentiation of delta and open marine deposits based on an integrated ichnological and sedimentological analysis of the Late Triassic Nayband Formation, Tabas Block, Central Iran. *Journal of Iberian Geology 43,* 413-437.

Besse, J., Torcq, F., Gallet, Y., Ricou, L., Krystyn, L. & Saidi, A. (1998). Late Permian to Late Triassic palaeomagnetic data from Iran: constraints on the migration of the Iranian block through the Tethyan Ocean and initial destruction of Pangaea. *Geophysical Journal International 135*, 77-92.

Bhattacharya JP (2006) Deltas. In H. W. Posamentier, & R. G. Walker (Eds.), Facies Models Revisited. *SEPM Special Publication 84*, 237-292.

Boggs, J. R. S. (2009). *Petrology of Sedimentary Rocks*. 2nd edn. Cambridge University Press

Bohacs, K. & Suter, J. (1997). Sequence stratigraphic distribution of coaly rocks: fundamental controls and paralic examples. *American Association of Petroleum Geologists Bulletin 81*, 1612-1639.

Brönnimann, P., Zaninetti, L., Bozorgna, F., Dashti, G. R. & Moshtaghian, A. (1971). Lithostratigraphy and foraminifera of the Upper Triassic Naiband Formation, Iran. *Revue de Micropaléontologie 14*, 7-16.

Burgess, D. T. (2014). *Early and Late Iron Diagensis in the Upper Triassic Shinarump Member of the Chinle Formation (Utah and Arizona).* Unpublished M.S. Thesis, University of Nebraska, Lincoln.

Burley, S. & Worden, R. (2003). *Sandstone diagenesis: Recent and ancient*. Reprint series of International Association of Sedimentologists, Blackwell Publishing Ltd.

Catuneanu, O. (2003). *Sequence Stratigraphy of Clastic Systems*. St. John's Newfoundland: Geological Association of Canada.

Chou, C. L. (2012). Sulfur in coals: A review of geochemistry and origins. *International Journal of Coal Geology 100*, 1-13.

Cifelli, F., Mattei, M., Rashid, H. & Ghalamghash, J. (2013). Right-lateral transpressional tectonics along the boundary between Lut and Tabas blocks (Central Iran). *Geophysical Journal International 193*, 1153-1165.

Cirilli, S., Buratti, N., Senowbari-Dariyan, B. & Fürsich, F. T. (2005). Stratigraphy and palynology of the Upper Triassic Nayband Formation of East-Central Iran. *Rivista Italiana di Paleomtologia e Stratigrafia 111*, 259-270.

Dai, S., Bechtel A., Eble, C. F., Flores, R. M., French, D., Graham, I. T., Hood, M. M., Hower, J. C., Korasidis, V. A., Moore, T. A., Püttmann, W., Wei, Q., Zhao, L. & O'Keefe, J. M. K. (2020). Recognition of peat depositional environments in coal: a review. *International Journal of Coal Geology 219*, 103383. https://doi.org/10.1016/j.coal.2019.103383.

Davis, R. A. (2012). Tidal signatures and their preservation potential in stratigraphic sequences. In R. A. Davis, & R. Dalrymple (Eds.), *Principles of Tidal Sedimentology* (pp. 35-55). Cham: Springer.

Davoudzadeh, M. & Schmidt, K. (1984). A review of the Mesozoic paleogeography and paleotectonic evolution of Iran. *Neues Jahrbuch für Geologie und Paläontologie, Abhandlungen 168*, 182-207.

Diessel, C. F. K. (1992). *Coal-Bearing Depositional Systems*. Cham: Springer.

Douglas, J. A. (1929). A marine Triassic fauna from eastern Persia. *The Quarterly Journal of the Geological Society of London 85*, 625-650.

Elliott, T. (1986). Deltas. In H. G. Reading (Ed.), *Sedimentary Environments and Facies* (pp. 113-154). Oxford: Blackwell.

Embry, A. F. & Klovan, J. E. (1971). A Late Devonian reef tract on Northeastern Banks Island, NWT. *Bulletin of Canadian Petroleum Geology 19*, 730-781.

Etesampour, A., Mahboubi, A., Moussavi-Harami, R., Arzani, N. & Bagi, H. A. (2020). Depositional history and sequence stratigraphy of central Tethyan from the Upper Triassic Nayband Formation, Central Iran. *Carbonates Evaporites 35*, 1-18. https://doi.org/10.1007/s13146-019-00540-0.

Fielding, C. R. (1987). Coal depositional models for deltaic and alluvial plain sequences. *Geology 15*, 661-664.

Flint, S., Aitken, J. & Hampson, G. (1995). Application of sequence stratigraphy to coal-bearing coastal plain successions: implications for the UK Coal Measures. In M. K. G. Whateley, & D. A. Spears (Eds.), European Coal Geology. *Journal of Geological Society of London Special Publication 82*, 1-16.

Folk, E. (1980). *Petrography of Sedimentary Rocks*. Austin: Hemphill Publishing Company.

Fürsich, F. T., Hautmann, M., Senowbari-Daryan, B. & Seyed-Emami, K. (2005). The Upper Triassic Nayband and Darkuh formations of East-Central Iran: stratigraphy, facies patterns and biota of extensional basins on an accreted terrane. *Beringeria 35*, 53-133.

Gastaldo, R. A., Demko, T. M. & Liu, Y. (1993). Application of sequence and genetic stratigraphic concepts to Carboniferous coal-bearing strata: an example from the Black Warrior Basin, USA. *Geologische Rundschau 82*, 212-226.

Ghassabiyan, N. N., Saidi, A., Aghanabati, A., Qorashi, M., Ghasemi, M. R. (2010). Geohistory analysis of the Tabas Block (Abdoughi-Parvadeh Basins) as seen from the Late Triassic through Early Cretaceous subsidence curves. *Islamic Republic of Iran Journal of science 21,* 49-63.

Ghavidel-Syooki, M., Yousefi, M., Shekarifard, A. & Mohnhoff, D. (2015). Palynostratigraphy, paleogeography and source rock evaluation of the Nayband Formation at the Parvadeh Area, Central Iran, Iran. *Islamic Republic of Iran Journal of Science 26*, 241-263.

Golonka, J. (2007). Late Triassic and Early Jurassic paleogeography of the world. *Palaeogeography, Palaeoclimatology, Palaeoecology 244*, 297-307.

Hagelskamp, H. H. B., Eriksson, P. G. & Snyman, C. P. (1988). The effect of depositional environment on coal distribution and quality parameters in a portion of the Highveld Coalfield, South Africa. *International Journal of Coal Geology 10*, 51-77.

Haq, B. U. (2018). Triassic Eustatic Variations Reexamined. *Geological Society of America 28*, 4-9.

Harms, J. C., Southard, J. B., Spearing, D. R. & Walker, R.G. (1975). Depositional environments as interpreted from primary sedimentary structures and stratification sequences. *SEPM Society for Sedimentary Geology*. https://doi.org/10.2110/scn.75.02.

Hautmann, M., Aghababalou, B. & Krystyn, L. (2011). An unusual Late Triassic nuculid bivalve with divaricate shell ornamentation, and the evolutionary history of oblique ribs in Triassic bivalves. *Journal of Paleontology 85*, 22-28.

Holz, M., Kalkreuth, W. & Banerjee, I. (2002). Sequence stratigraphy of paralic coal-bearing strata: an overview. *International Journal of Coal Geology 48*, 147-179.

Ketzer, J. M., Holz, M., Morad, S. & Al-Aasm, I. S. (2003). Sequence stratigraphic distribution of diagenetic alterations in coal-bearing, paralic sandstones: Evidence from the Rio Bonito Formation (Early Permian), Southern Brazil. *Sedimentology 50*, 855-877.

Kluyver, H. M., Tirrul, R., Chance, P. N., Johns, G. W. & Meixner, H. M. (1983). Explanatory text of the Naybandan Quadrangle Map 1: 250,000. *Geological Survey of Iran, Quadrangle J8*, 1-43.

Konon, A., Nadimi, A., Koprianiuk, M., Wysocka, A., Szaniawski, R., Wygladala, M., Slaby, E., Beygi, S. & Barski, M. (2016). Formation of intracontinental basins in the opposite corners of the Tabas block as coeval structures controlled by transpressional faulting, Iran. *Geological Society of America Bulletin 128*, 1593-1617.

Krystyn, L., Balini, M., Sepehriannasa Aghababalou, B. & Hairapetian, V. (2019). Norian ammonoids from the Nayband Formation (Iran) and their bearing on late Triassic sedimentary and geodynamic history of the Iran plate. *Rivista Italiana di Paleontologia e Stratigrafia 125*, 231-248.

Li, W., Bhattacharya, J. P., Zhu, Y. & Garza, D. (2011). Evaluating delta asymmetry using three-dimensional facies architecture and ichnological analysis, Ferron 'Notom Delta' Capital Reef, Utah, USA. *Sedimentology 58*, 478-507.

Littke, R. & Zieger, L. (2019). Deposition, diagenesis and petroleum generation potential of Pennsylvanian coals and coal-bearing strata in Western Germany: a review. *Zeitschrift der Deutschen Gesellschaft für Geowissenschaften 170*, 289-309.

MacEachern, J. A. & Gingras, M. K. (2007). Recognition of brackish-water trace fossil assemblages in the Cretaceous western interior seaway of Alberta. In R. G. Bromley, L. A. Buatois, M. G. Mangano, J. F. Genise, & R. N. Melchor (Eds.), Sediment-Organism Interactions; A Multifaceted Ichnology. *SEPM Special Publication 88*, 49-194.

McCabe, P. J. (1993). Sequence stratigraphy of coal-bearing strata. In J. A. Breyer, A. W. Archer. & P. J. McCabe (Eds.), *Sequence Stratigraphy of Coal-Bearing Strata* (pp. 1-50). Tulsa: AAPG Field Trip Guidebook and Short Course Supplement.

Miall, A. D. (2000). *Principals of Sedimentary Basin Analysis. 3rd editon*. Cham: Springer.

Miall, A. D. (2006). *The Geology of Fluvial Deposits, Sedimentary Facies, Bastion Analysis and Petroleum Geology. 4th editon*. Cham: Springer.

Nützel, A. & Senowbari-Daryan, B. (1999). Gastropods from the Late Triassic (Norian-Rhaetian) Nayband Formation of Central Iran. *Beringeria 23*, 93-132.

Repin, U. (1996). New Late Triassic bivalves from Iran and a taxonomy of the superfamily Spondylacea. *Paleontological Journal 30*, 363-369.

Ryer, T. A. (1983). Transgressive-regressive cycles and the occurrence of coal in some Upper Cretaceous strata of Utah. *Geology 2*, 207-210.

Sabbaghiyan, H., Aria-Nasab, M. & Ghasemi-Nejad, E. (2020). The palynology of the Nayband Formation (Upper Triassic) of the Tabas Block, Central Iran. *Review of Paleobotany and Palynology 282*, https://doi.org/10.1016/j.revpalbo.2020.104308.

Saidi, A., Brunet, M. F. & Ricou, L. E. (1997). Continental accretion of the Iran Block to Eurasia as seen from Late Paleozoic to Early Cretaceous subsidence curves. *Geodinamica Acta 10*, 189-208.

Sajjadi, F., Hashemi, H. & Borzuee, E. (2015). Palynostratigraphy of the Nayband Formation, Tabas, Central Iran Basin: paleogeographical and paleoecological implications. *Journal of Asian Earth Sciences 111*, 553-567.

Salehi, M. A., Mousavi-Harami, S. R., Mahboubi, A. & Rahimi, B., (2015). Lithofacies and depositional environment of the Early Jurassic Ab-Haji Formation in outcrop and exploration boreholes of Parvadeh Coal Mine, Tabas, East Central Iran. *Scientific Quarterly Journal, Geosciences 24* (94), 249-262. [in Persian]

Scott, A. C. (1989). Deltaic coals: An ecological and palaeobotanical perspective. In M. K. G. Whateley, & K.T. Pickering (Eds.), *Deltas: Sites and Traps from Fossil Fuels. Geological Society Special Publication 41*, 309-316.

Seyed-Emami, K. (2003). Triassic in Iran. *Facies 48*, 91-106.

Seyed-Emami, K., Fürsich, F. T. & Wilmsen, M. (2004). Documentation and significance of tectonic events in the Northern Tabas block (East-Central Iran) during the Middle and Late Jurassic. *Rivista Italiana di Paleontologia e Stratigrafia 110*, 163-171.

Seyed-Emami, K., Fürsich, F. T. & Wilmsen, M. (2005). New Evidence on the Lithostratigraphy of the Jurassic System in the Northern Tabas Block, East-Central Iran. *Geosciences 15*, 7897. [in Persian]

Shariat Nia, H. (1994). Geological characteristics of the Parvadeh Region of the Tabas coal-bearing basin, Central Iran. *Canadian Society of Petroleum Geologists 17*, 497-509.

Shariat Nia, M. H., Mohammadi, A. R. & Motevali Haghi, S. A. (1997). *Exploration report of Parvadeh coal-bearing area (general information)*. National Iranian Steel Company, Unpublished report. [in Persian]

Shiers, M. N., Hodgson, D. M. & Mountney, N. P. (2017). Response of a coal-bearing coastal-plain succession to marine transgression: Campanian Neslen Formation, Utah. U.S.A., *Journal of Sedimentary Research 87*, 168-187.

Stock, A. T., Littke, R., Lücke, A., Zieger, L. & Thielemann, T. (2016). Miocene depositional environment and climate in western Europe: the lignite deposits of the Lower Rhine Basin, Germany. *International Journal of Coal Geology 157*, 2-18.

Stöcklin, J. (1974). Possible ancient continental margin in Iran, In C. A Burke. & C. L. Drake (Eds.), *The Geology of Continental Margins* (pp. 873-887). New York: Springer.

Stow, D. A. V. (1981). Fine-grained sediments: terminology. *Quarterly Journal of Engineering Geology and Hydrogeology, London 14*: 243-244.

Takin, M. (1972). Iranian geology and continental drift in the Middle East. *Nature 235*: 147-150.

Thomas, L. (2002). *Coal Geology. 2nd edition*. Chichester: Wiley-Blackwell, John Wiley and Sons.

Tucker, M. E. (2001). *Sedimentary Petrology. 3rd edition*. Oxford: Blackwell.

Vaez-Javadi, F. (2012). Biostratigraphy of Nayband Formation in Tabas, Parvadeh coal mine, according to botanical macrofossils. *Journal of Stratigraphy and Sedimentology Researches 46*(1), 113-143. [in Persian]

Vassilev, Y. (1984). *Mesozoic flora fossils of Iran's coal-bearing areas*. National Iranian Steel Company, Unpublished report.

Vassilev, S. V. & Vassiliva, C. G. (1996). Occurrence, abundance and origin of minerals in coals and coal ashes. *Fuel Processing Technology 48*, 85-106.

Wilmsen, M., Fürsich, F. T., Seyed-Emami, K. & Majidifard, M. R. (2009a). An overview of the stratigraphy and facies development

of the Jurassic System on the Tabas Block, East-Central Iran. *Geological Society London Special Publication 312*, 323-343.

Wilmsen, M., Fürsich, F. T., Seyed-Emami, K., Majidifard, M. R. & Taheri, J. (2009b). The Cimmerian orogeny in northern Iran: tectono-stratigraphic evidence from the foreland. *Terra Nova 21*, 211-218.

Worden, R. H. & Morad, S. (2003). *Clay Mineral Cements in Sandstones*. Hoboken: Wiley-Blackwell.

Wright, L. D. (1985). River deltas. In R. A. Davies (Ed.), *Coastal Sedimentary Environments* (pp. 1-76). New York: Springer.

Zamaniyan, E., Khanehbad, M., Moussavi-Harami, R. & Mahboubi, A. (2018). Lithofacies and sedimentary environment of Qadir member of the Nayband Formation on Parvadeh Coal Mine region, East-Central of Iran. *Geosciences Quarterly Journal 28*, 295-304. [in Persian]

Zamansani, N., Rajabzadeh, M.A., Littke, R., Zieger, L. & Baniasad, A. (2019). Organic petrology and geochemistry of Triassic and Jurassic coals of the Tabas Basin, Northeastern/Central Iran. *International Journal of Coal Science and Technology 6*, 354-371.